

2006

Characterization of the temperature dependence of the index of refraction and the thermo-optic coefficient for infrared materials

Christopher J. DiRocco
University of Dayton

Follow this and additional works at: https://ecommons.udayton.edu/graduate_theses

Recommended Citation

DiRocco, Christopher J., "Characterization of the temperature dependence of the index of refraction and the thermo-optic coefficient for infrared materials" (2006). *Graduate Theses and Dissertations*. 2359.
https://ecommons.udayton.edu/graduate_theses/2359

This Thesis is brought to you for free and open access by the Theses and Dissertations at eCommons. It has been accepted for inclusion in Graduate Theses and Dissertations by an authorized administrator of eCommons. For more information, please contact mschlangen1@udayton.edu, ecommons@udayton.edu.

**CHARACTERIZATION OF THE TEMPERATURE DEPENDENCE OF THE
INDEX OF REFRACTION AND THE THERMO-OPTIC
COEFFICIENT FOR INFRARED MATERIALS**

Thesis

Submitted to

The School of Engineering of the
UNIVERSITY OF DAYTON

in Partial Fulfillment of the Requirements for

The Degree

Master of Science in Electro-Optics

by

Christopher J. DiRocco

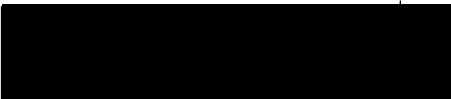
UNIVERSITY OF DAYTON

Dayton, Ohio

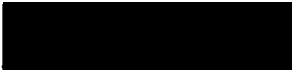
May, 2006

**Characterization of the Temperature Dependence of the Index of Refraction
and the Thermo-optic Coefficient for Infrared Materials**

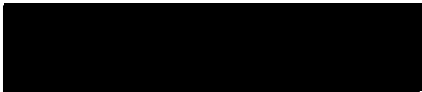
APPROVED BY:



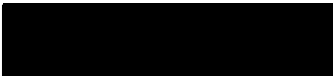
✓ Peter E. Powers, Ph.D.
Professor,
Electro-Optics Program
University of Dayton
Committee Chairman



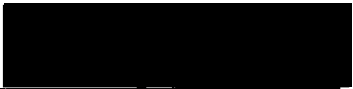
Glen Gillen, Ph.D.
Optical Research Scientist
Materials Directorate
Air Force Research Lab
Committee Member




✓ Joseph W. Haus, Ph.D.
Professor,
Electro-Optics Program
University of Dayton
Committee Member



✓ Shekhar Guha, Ph.D.
Principal Scientist
Materials Directorate
Air Force Research Lab
Committee Member



Donald L. Moon, Ph.D.
Associate Dean
Graduate Engineering Programs
& Research
School of Engineering



✓ Joseph E. Saliba, Ph.D., P.E.
Dean
School of Engineering

Abstract

CHARACTERIZATION OF THE TEMPERATURE DEPENDENCE OF THE INDEX OF REFRACTION AND THE THERMO-OPTIC COEFFICIENT FOR INFRARED MATERIALS

Christopher J. DiRocco
University of Dayton

Advisor: Dr. Peter E. Powers

The effect of temperature changes on the index of refraction of optical materials is very important to optical device applications. Without an accurate knowledge of a material's index of refraction and thermo-optic coefficient, thermal changes of the material's physical and optical properties can become the source of errors in many applications especially ones dealing with nonlinear light-matter interactions.

In the past, refractive index measurements have been conducted at room and cryogenic temperatures using a modified Michelson interferometer for wafer-shaped infrared materials. Other general methods for index measurements have been conducted for various material shapes including the minimum deviation method, ellipsometry, immersion, and other interferometric designs.

In this thesis, an angle-dependent Michelson/Fabry-Perot interferometer, a temperature-dependent Fabry-Perot interferometer, and a temperature-dependent optical micrometer are used to accurately measure the temperature dependent index of refraction and thermo-optic coefficient of wafer-shaped

optical materials. These measurements were validated against known materials and then extended to materials where no previous knowledge of the thermal properties were known. An advantage of the techniques used in this thesis is that they are non-destructive in nature.

Using this technique, the temperature-dependent index of refraction and thermo-optic coefficient were measured at a laser wavelength of 10.591 μm for the approximate temperature ranges of 100 to 350 K for Ge, Si, InAs, and 100 to 200 K for InSb. The thermal expansion coefficients and thermo-optic coefficients of Ge and Si have been previously well documented for the temperature range 98-298 K and were used to verify these methods and results. To the best of our knowledge these are the first experimentally reported results for InAs and InSb across the noted temperature ranges.

Acknowledgments

I would like to thank Dr. Glen Gillen, Mr. Leo Gonzalez, Dr. Shekhar Guha, and the rest of the IR lab team at the Air Force Research Lab for their constant and invaluable advice, answers, questions and overall guidance on this project. I would also like to thank my advisor Dr. Peter Powers from the University of Dayton for his help in keeping me on track with my research and thesis preparation.

Table of Contents

Abstract.....	iii
Acknowledgments.....	v
Table of Contents.....	vi
List of Illustrations	x
List of Tables	x
Chapter 1 Introduction	1
1.1 Background	1
1.2 Problem Statement.....	1
1.3 Research Objective	2
1.4 Methodology	3
Chapter 2 Background and Refractive Index Measurements.....	4
2.1 Refractive Index, A Brief Review	4
2.2 Different Methods of Measurement	5
2.3 Project Goal Restrictions	8
2.4 Method Choice	8
Chapter 3 Experimental Theory	11
3.1 Slope of the nL versus Temperature Theory	11
3.2 Absolute Value of Optical Path Length Theory	14
3.3 Temperature Dependent Thickness Measurements Theory.....	15
3.4 Final Calculations using Three Experiments.....	16
Chapter 4 Slope of the Optical Path Length vs. Temperature Measurement.....	17
4.1 Experimental Design	17
4.1.1 Michelson Interferometer	17
4.1.2 Fabry-Perot Interferometer using Michelson Design.....	19
4.1.3 Fabry-Perot Interferometer.....	20
4.2 Testing System Accuracy	24
Chapter 5 Absolute Value of the Index of Refraction	26
5.1 Room Temperature Index of Refraction Measurement.....	26
5.2 Experimental Method.....	28
5.3 Cryogenic Temperature Index of Refraction Measurement	32
Chapter 6 Thermal Expansion Coefficient and Absolute Thickness Measurements	34
6.1 LaserMike Optical Micrometer	34
6.2 Absolute Thickness Measurements.....	34
6.3 Temperature Dependent Thickness Measurements	36
Chapter 7 Results	40
7.1 Angle Dependent Michelson/Fabry Interferometer Data.....	41

7.2	LaserMike Optical Micrometer Data	43
7.3	Temperature Dependent Fabry-Perot Data	45
7.4	Final Results and Discussion.....	47
Chapter 8	Conclusions.....	54
8.1	Accomplishments	55
8.2	Future Goals.....	57
References	59

List of Illustrations

Figure 3.1: 1 st and 2 nd transmitted beams through a flat parallel sample.	12
Figure 4.1: Temperature-dependent Michelson interferometer.....	18
Figure 4.2: Output signal vs. temperature for Ge using Michelson interferometer.	19
Figure 4.3: Output signal vs. temperature for Ge using Michelson interferometer as Fabry-Perot interferometer.....	20
Figure 4.4: Temperature-dependent Fabry-Perot interferometer design.....	21
Figure 4.5: Output signal vs. temperature for Ge using Fabry-Perot interferometer.	23
Figure 4.6: Uncorrected nL vs. temperature for Ge using Fabry-Perot interferometer.	23
Figure 4.7: nL vs. temperature compared to two other studies.....	25
Figure 5.1: Design for Michelson/Fabry-Perot interferometer.	27
Figure 5.2: Output signal vs. angle for Michelson interferometer using InAs.	29
Figure 5.3: Output signal vs. angle for Fabry-Perot interferometer using InAs. ..	30
Figure 5.4: Phase vs. angle for Michelson interferometer using InAs.	31
Figure 5.5: Phase vs. angle for Fabry-Perot interferometer using InAs.	31
Figure 5.6: Phase difference and Michelson and Fabry-Perot phases vs. angle using InAs.....	32
Figure 5.7: Temperature and angle-dependent Michelson/Fabry-Perot interferometer.	33
Figure 6.1: LaserMike optical micrometer setup for room temperature measurements.	35
Figure 6.2: LaserMike optical micrometer design for room and cryogenic temperature measurements.....	37
Figure 7.1: nL vs. temperature for Ge.....	46
Figure 7.2: nL vs. temperature for Si.....	46
Figure 7.3: nL vs. temperature for InAs.....	47
Figure 7.4: nL vs. temperature for InSb.	47
Figure 7.5: n vs. temperature for Ge.....	50
Figure 7.6: n vs. temperature for Si.....	50
Figure 7.7: n vs. temperature for InAs.....	51
Figure 7.8: n vs. temperature for InSb.	51
Figure 7.9: dn/dT vs. temperature for Ge.....	52
Figure 7.10: dn/dT vs. temperature for Si.	52

Figure 7.11: dn/dT vs. temperature for InAs.	53
Figure 7.12: dn/dT vs. temperature for InSb.	53
Figure 7.13: dn/dT vs. temperature for Ge using two methods.	54
Figure 8.1: Future setup for both interferometers.	58

List of Tables

Table 7.1: Index and thickness measurements for Ge and Si using Michelson/Fabry-Perot.....	41
Table 7.2: Index and thickness measurements for InAs using Michelson/Fabry- Perot.	42
Table 7.3: Index and thickness measurements for InSb using Michelson/Fabry- Perot.	43
Table 7.4: Linear thermal expansion coefficient data.....	43
Table 7.5: Accuracy of linear thermal expansion calculations.....	44
Table 7.6: Temperature dependent thickness equations.	45
Table 7.7: n vs. temperature function coefficients.....	52
Table 7.8: dn/dT vs. temperature function coefficients.....	54
Table 8.1: Possible setups using two laser design for project.....	58

Chapter 1

Introduction

1.1 Background

Knowing the effect of temperature changes on the index of refraction (n) of optical materials is very important for optical applications. Without an accurate knowledge of a material's index of refraction and thermo-optic coefficient (dn/dT), thermal changes of the material's physical and optical properties can become the source of errors in many applications especially ones dealing with nonlinear light-matter interactions.

In the past, refractive index measurements have been conducted at room and cryogenic temperatures using a modified Michelson interferometer for wafer-shaped infrared materials^{1,2}. Other general methods for index measurements include the minimum deviation method, ellipsometry, immersion, and other interferometric designs.

1.2 Problem Statement

The development of an experiment that can measure the index of refraction across the entire temperature range of cryogenic to room temperature

would vastly increase the accuracy of theoretical calculations done in which the value of the refractive index is needed. For example, predicting a specific crystal cut and temperature for second harmonic generation of an infrared laser is critically dependent on the index of refraction. Moreover, it is desirable that this experiment measure the index of refraction and thermo-optic coefficient without damaging the sample. A major challenge for measuring optical properties of infrared material is due to their limited size. Semiconductors and infrared materials are typically grown as thin wafers or in boules where they are subsequently sliced into thin flat samples.

Another important requirement is that the measurement can be made without any previously known knowledge of the material; i.e., physical thickness or thermal expansion coefficient. Having a reliable and accurate technique of determining optical properties of unknown materials may also be useful in the identification of materials.

1.3 Research Objective

The objective of this research is to create an experiment to independently measure the index of refraction (n) and thickness (L) of a material across the approximate temperature range of 77-350 K using a wavelength tunable CO₂ laser at wavelength 10.591 μm . As the experiment developed it was decided that the focus of the project would be on measuring the temperature dependence of n and the thermo-optic coefficient, dn/dT . The results of this data would allow for a greater knowledge of the studied materials' properties and therefore allow for a more accurate use of these materials in future experiments and theoretical

calculations which depend upon temperature. Eventually, this experiment would also be integrated with different laser sources such that it could provide a fuller and more accurate Sellmeier equation for each material studied as well.

1.4 Methodology

The relationship between the index of refraction, thickness, and temperature was obtained using a combination of a temperature-dependent Fabry-Perot interferometer, an angle-dependent Michelson and Fabry-Perot interferometer, and a temperature-dependent optical micrometer. In all three cases, data was collected with a specifically designed data acquisition program (Labview) and interpreted and analyzed using specifically designed analysis programs (using Igor Pro 4.0). Compiling the data from all three experiments provides enough information to create a polynomial function to describe the effective index of refraction and thermo-optic coefficient across the studied temperature range.

Chapter 2

Background and Refractive Index Measurements

2.1 *Refractive Index, A Brief Review*

As light transverses a boundary between media of different optical properties at a non-normal angle, the speed of the wave and the propagation direction change. This is known as refraction. The bending of the wave (Snell's Law) is caused by the difference in wave speed between two materials. The refractive properties of light in a material are determined by its refractive index. The absolute index of refraction of a material is a dimensionless number defined as

$$n = \sqrt{\frac{\epsilon\mu}{\epsilon_0\mu_0}} = \frac{c}{v} \quad (2.1)$$

where ϵ and μ are the permittivity and permeability of the medium, ϵ_0 and μ_0 are the permittivity and permeability of free space, c is the speed of light in a vacuum, and v is the velocity of propagation through the material³. Hence, the larger the index of refraction, the slower light propagates through a material.

The wavenumber, k , which describes electromagnetic wave propagation is dependent on the refractive index of the medium through the relation

$k = 2\pi m/\lambda$. This makes n an important parameter in electromagnetic propagation and light-matter interactions. For this reason, it is important to know both the value of the index of refraction and the effect of different variables on which n is dependent; for example, the wavelength of the incident radiation and the material's temperature.

2.2 *Different Methods of Measurement*

Various measurement techniques for the index of refraction for optical materials have been developed and improved for many years. These methods include the minimum deviation method⁴, ellipsometry⁵, immersion⁶, and interferometry⁷. Index values have also been theorized using mathematical models based upon other fundamental parameters of the material. Each technique and their limitations and applications will be briefly described here.

In the minimum deviation method, or prism method, a prism of sample is created. The prism is then rotated until the angular deviation of an incident laser beam passing through the prism is minimized. Using Snell's law and the known angle of incidence, the index of refraction can be calculated from the angle of minimum deviation and the prism's apex angle³. Other techniques such as the "fixed angle of incidence method" exist as slight variations on this classic method⁸. The technique of minimum deviation is very accurate at room temperature and is generally used for measuring the wavelength dependence of the refractive index⁴. For other temperatures, especially cryogenic ones, it can become experimentally challenging. A second limitation is that it requires a relatively large quantity of the sample for the prism to be manufactured. Overall,

this is a very good technique for measuring the index of refraction for common materials at room temperature.

Ellipsometry exploits the subtle differences in the reflection coefficients between s and p -polarized light by reflecting light off a thin film (nm- μ m thick) of sample to measure the index of refraction⁵. Reflecting light off a thin film produces two sources of light, the reflection off the surface of the film and the reflection off the back surface of the film. The phase of the second mentioned beam is dependent on the refractive index of the material. The index is discerned by measuring the reflectance of the s and p polarizations for both reflections. This technique is accurate for room temperature, but is difficult to setup for other temperatures and requires detection equipment capable of measuring very small changes in the polarization direction of the reflected beam. It also requires a very small quantity of material, i.e. a thin film. This can be either an advantage or disadvantage based on the situation. Applications of this technique include the accurate thickness and index measurements of thin films and the identification of materials and thin layers.

A third technique used for measuring the index of refraction is immersion^{6,9}. In this case, a material is immersed in an oil of known temperature-dependent refractive index. Light is then passed through the oil and the sample material, and the temperature of the oil is varied. If the refractive indices of the oil and sample are equal, the light will be unaffected as it passes from one to the other and no surface scattering will occur. Multiple oils exist having many different refractive index ranges for use with various optical

materials. This method is also useful for measuring the index of samples that are randomly shaped. They do not need to be polished, flat parallel, large, or small. The disadvantage to this method is that the range of indices available for immersion oils is limited, though new oils are being created all the time⁹. Another disadvantage is in measuring the index as a function of wavelength or temperature. It is unlikely that the oil and material under test would have the same dispersion properties.

Interferometric techniques are often used to measure the temperature dependent index of refraction and thickness of a material. Interferometric studies involve analysis of the interference pattern created by temperature variations to the change in the optical path length through the material. Specifically, the change in temperature between any two constructive or destructive peaks is measured to create a relationship between temperature, thickness, and the index of refraction^{7,10,11,12}. After these general similarities though, many variations in the exact setup design occur due to specific restrictions existent in the system or measurement requirements or constraints, such as not destroying the sample. Interferometry requires a polished flat parallel sample for study. A wedged sample may be used in certain cases, though it provides many added difficulties. Based on the design, interferometry can be used for measurements of the refractive index, the material's thickness, the thermal expansion coefficient, or the thermo-optic coefficient.

Finally, many mathematical models have been built to theorize the value of the refractive index. These models include approaches such as using the

Penn model to define the electronic contribution¹³ to the dielectric constant or combining the general theory of dispersion and the well-known Kramers-Kronig relationship¹⁴. In comparison to other techniques, modeling can be less accurate but it is useful for collecting rough estimates of n for materials and temperatures not previously studied by others.

2.3 *Project Goal Restrictions*

It is clear that there are many ways to measure the refractive index of a material. The choice of experimental design is dependent on the project goals and restrictions. The goal of this experiment is to measure n and dn/dT of a semiconductor material for all temperatures between room and cryogenic.

One restriction is that this has to be done without causing any damage to the samples. The specific samples studied in this project are infrared materials typically grown as thin flat parallel wafers. Therefore, flat parallel wafers are the only available sample shape.

Measuring the index across a temperature range provides many challenges as well. The sample studied must be held in a dewar kept at vacuum to prevent condensation as temperature is lowered. This means adjustments to the sample itself are limited once under vacuum.

Finally, the temperature dependence of thickness is also a major restriction. Both n and L are independently affected by temperature. This project is designed such that the change in thickness with temperature can be decoupled from the temperature dependent refractive index measurements. It

also does not require the thickness or thermal expansion coefficient to be previously known.

2.4 Method Choice

It was decided that interferometry was the best method for this project. This was due to many reasons. First, interferometry had been used previously in this lab to measure n values at room and cryogenic temperatures^{1,2} and the experimental setups still existed. Second, this technique is easily adjusted to work at a set temperature or to work with varying temperatures. While a second experiment is needed to set the absolute value measurements of n at a specific temperature, interferometry is still the best choice for this measurement. This is because one purpose of this project was to have an experiment ready to measure the index of refraction for newly created samples. These new wafer shaped materials do not have enough material available for the prism method and simultaneously have too much material for ellipsometry. Only one flat parallel wafer is needed for all experiments used in this project if interferometry is used. Finally, the immersion method could not be used for absolute index measurements, as there are no oils available with refractive indices near 4.0, a rough index value for many semiconductors.

There are many system variables and choices available when using interferometry for measuring temperature dependent n and dn/dT . In comparison to other previous studies, this project focused on a couple of specific issues.

One problem with past techniques is that they required the absolute value of the index of refraction at some temperature or the thermal expansion

coefficient to calculate the n and dn/dT across a temperature range¹². The interferometric technique used in this project is also not by itself sufficient to determine unambiguously n and dn/dT . However, our laboratory contains the setups needed to calculate these values as well such that no previous knowledge is needed for any sample studied with the project.

A second difference between other past techniques and this project's is that the majority of previous research has been done above room temperature^{7,11,12}. The measurement theory used above room temperature is the same as below but very few people have studied the effects of cold on materials in comparison to the effect of heat. In practice, making cryogenic measurements just requires a nitrogen cooled housing for the sample instead of a furnace heated housing.

One final issue is that the samples used could not be harmed or destroyed in any way. One previous technique used the interference of the beam reflected off the front and back surface of a flat polished sample in a heater to measure the thermal expansion and thermo-optic coefficients above room temperature⁷. To measure both dn/dT and α with one experiment, this design involved cutting a hole in the sample to add a third set of data by also recording the reflection off the location of the back surface of the sample (through the hole). While this was a valid way to measure both values, it involved damaging the sample.

Chapter 3

Experimental Theory

With all the goals and restrictions existent in this project, it was decided that no one experiment would produce all the data needed to calculate the temperature dependent n and dn/dT . This conclusion led to the creation of three separate goals with three separate experiments. These goals are the measurement of the slope of an optical path length (nL) versus temperature plot, the measurement of the absolute value of the index of refraction and thickness, and the measurement of the temperature-dependent thermal expansion coefficient and temperature dependent thickness. This chapter describes the general theory for each.

3.1 Slope of the nL versus Temperature Theory

The temperature-dependent nL is measured using the output signal versus temperature plot of a temperature-dependent Fabry-Perot interferometer. The relationship to nL is derived from the common equation for the phase change in a Fabry-Perot interferometer,

$$\phi_f(T) = 2kL \cos \theta_t = \frac{4\pi nL}{\lambda} \cos \theta_t, \quad (3.1)$$

where λ is the wavelength of the input laser beam, θ_t is the angle of refraction, k is the wave number, and $\phi_f(T)$ is the temperature dependent phase change between the first and second transmitted beams through the sample where one path has traversed the sample two or more times due to internal reflections¹⁵.

Figure 3.1 show the first two beam paths that interfere in this setup.

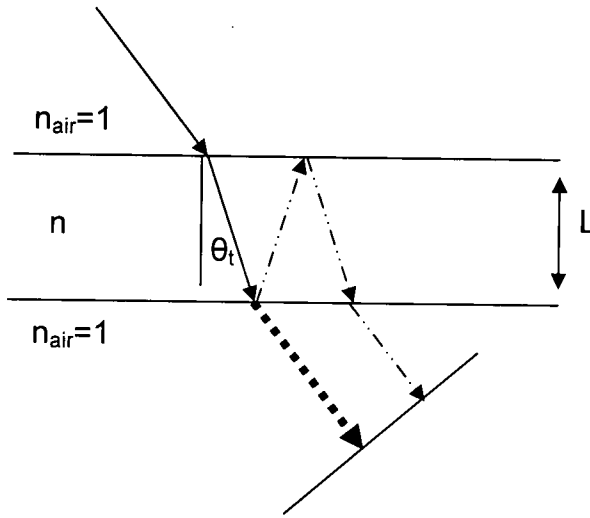


Figure 3.1: 1st and 2nd transmitted beams through a flat parallel sample.

The phase difference between the first and second transmitted beams can be found using Equation (3.1). Each successive transmission path (having two more internal reflections) will have the same phase difference with respect to the previous transmission path. The output of the etalon is the interference of an infinite number of beams with integer multiples of the same phase difference.

If the setup is created such that the angle of incidence is approximately zero, then the equation can be simplified to

$$\phi_f(T) = \frac{4\pi m(T)L(T)}{\lambda}. \quad (3.2)$$

This is also the equation for a Michelson interferometer in which the angle of incidence is approximately zero. The phase difference between an arbitrary number of constructive to destructive peak changes is πm where m is the number of changes. The change in the optical path length $\Delta(nL)$ between m peak to valley changes can then be calculated as

$$\pi m = \frac{4\pi \Delta(nL)_m}{\lambda}, \quad (3.3)$$

or

$$\Delta(nL)_m = m \frac{\lambda}{4}. \quad (3.4)$$

The change between $m+1$ peak to valley changes is therefore

$$\Delta(nL)_{m+1} = (m+1) \frac{\lambda}{4}. \quad (3.5)$$

Finally, the change in optical path length between an adjacent constructive and destructive peak is

$$\Delta(nL) = (m+1) \frac{\lambda}{4} - m \frac{\lambda}{4}, \quad (3.6)$$

or

$$\Delta(nL) = \frac{\lambda}{4}. \quad (3.7)$$

A combination of this simple equation and the output signal versus temperature plot yields an nL versus temperature plot. This plot is created by noting the temperature in which every constructive peak and destructive peak occurs and then setting the change in nL between every peak to be a quarter of the incident

laser wavelength, as denoted by Equation (3.7). In truth, this is not truly an nL versus temperature plot though. Equation (3.7) above only dictates the *change* in the optical path length between a constructive and destructive peak. It provides no information about the absolute value of nL at any location. For this reason, a second experiment is conducted to find the absolute value.

3.2 Absolute Value of Optical Path Length Theory

The absolute value of nL is an exact value of the optical path length at one specific temperature. To measure nL at some temperature, both n and L are calculated independently. This is done using angle-dependent Michelson and Fabry-Perot interferometers.

The theory behind this measurement is derived from two basic equations, the angle dependent phase difference for a Fabry-Perot interferometer¹,

$$\phi_f(\theta) = \frac{4\pi L}{\lambda} \sqrt{n^2 - \sin^2 \theta}, \quad (3.8)$$

and the angle dependent phase difference for a Michelson interferometer¹,

$$\phi_m(\theta) = \frac{4\pi L}{\lambda} \left(\sqrt{n^2 - \sin^2 \theta} + 1 - \cos \theta \right), \quad (3.9)$$

where θ is the angle of incidence on the sample. Both equations are dependent on thickness and index of refraction. By subtracting Equation (3.8) from Equation (3.9),

$$\phi_m(\theta) - \phi_f(\theta) = \frac{4\pi L}{\lambda} (1 - \cos \theta), \quad (3.10)$$

an equation independent of index of refraction is obtained. With the sample thickness measured, the index of refraction can be determined from either

Equation (3.8) or Equation (3.9). In cases where the fringe visibility of the Fabry-Perot interferometer is too weak, Equation (3.9) may be used to solve for the index of refraction if the absolute thickness at room temperature has been measured using some other approach such as a LaserMike optical micrometer.

3.3 Temperature Dependent Thickness Measurements Theory

The final goal is to measure the temperature dependence of a material's thickness. This is accomplished using an optical micrometer to measure the thickness of a material at different temperatures. The general equation for thickness as a function of temperature is

$$L(T) = L_{298} [1 + \alpha(T - 298)], \quad (3.11)$$

where L_{298} is the thickness at 298 K, T is the sample temperature, and α is the linear thermal expansion coefficient. If two sets of data are taken, cryogenic and room temperature, L_{298} can be removed using substitution. This yields an equation for the linear thermal expansion coefficient in terms of the thickness and temperatures at the two measurements,

$$\alpha = \frac{[L(T_2) - L(T_1)]}{[L(T_1) * (T_2 - 298) - L(T_2) * (T_1 - 298)]}, \quad (3.12)$$

where $T_2 > T_1$. Collecting multiple sets of data at both room and cryogenic temperatures provides a number of thermal expansion coefficient measurements to decrease experimental error. Once α has been accurately measured, the L_{298} can be calculated using the absolute thickness and temperature readings taken for one set temperature.

3.4 Final Calculations using Three Experiments

Once the optical path length and thickness versus temperature sets of data have been collected, the temperature dependent refractive index is easily calculated. This is done using the equation,

$$n(T) = \frac{(nL)(T)}{L(T)}. \quad (3.13)$$

The thermo-optic coefficient may be calculated from $n(T)$ since it is simply its derivative.

Chapter 4

Slope of the Optical Path Length vs. Temperature Measurement

4.1 *Experimental Design*

The first goal in this project was to record the temperature dependence of the optical path length, nL . This could be done using an interferometer. Hence, the first step was to consider which interferometric design would best provide the information needed. This led to trying three different designs, a Michelson interferometer, a Michelson-designed interferometer used as a Fabry-Perot, and a Fabry-Perot interferometer.

4.1.1 *Michelson Interferometer*

A Michelson interferometer was originally chosen as the design for this part of the experiment. The experimental setup consisted of a Michelson interferometer similar to the diagram in Figure 4.1. The sample is placed in a temperature controlled dewar in the path of one of the two beam arms. The effect of this setup is that the only changing variable in the path difference between the two arms is the effect of temperature on the sample. Hence, the

interference pattern created by the two arms of the Michelson is completely temperature dependent. This assumes the sample beam hits the sample at normal incidence and the sample surfaces are perfectly flat and parallel such that refraction has no effect.

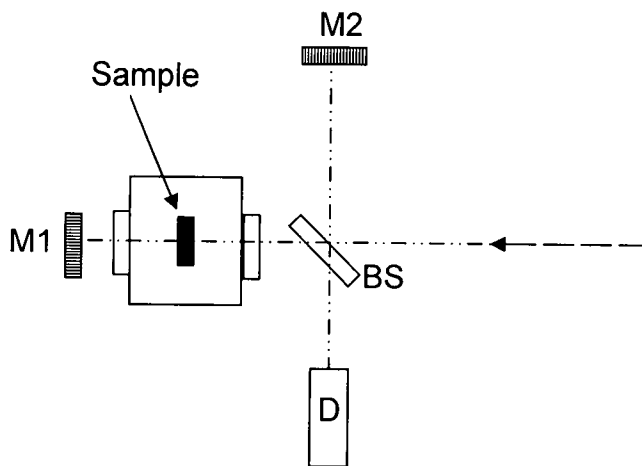


Figure 4.1: Temperature-dependent Michelson interferometer.

Figure 4.2 shows a plot of the temperature-dependent output of the Michelson setup. It was decided that due to a lack of clarity in the peak and valley locations in this plot, the Fabry-Perot interferometer should indeed be tested as well. Specifically, the exact location of the destructive interference peaks was unclear. It should be noted that the problems with the Michelson setup could have been fixed with alignment. The choice to try a Fabry-Perot setup was primarily due to the simplicity of alignment for a system that would be heavily used for this project.

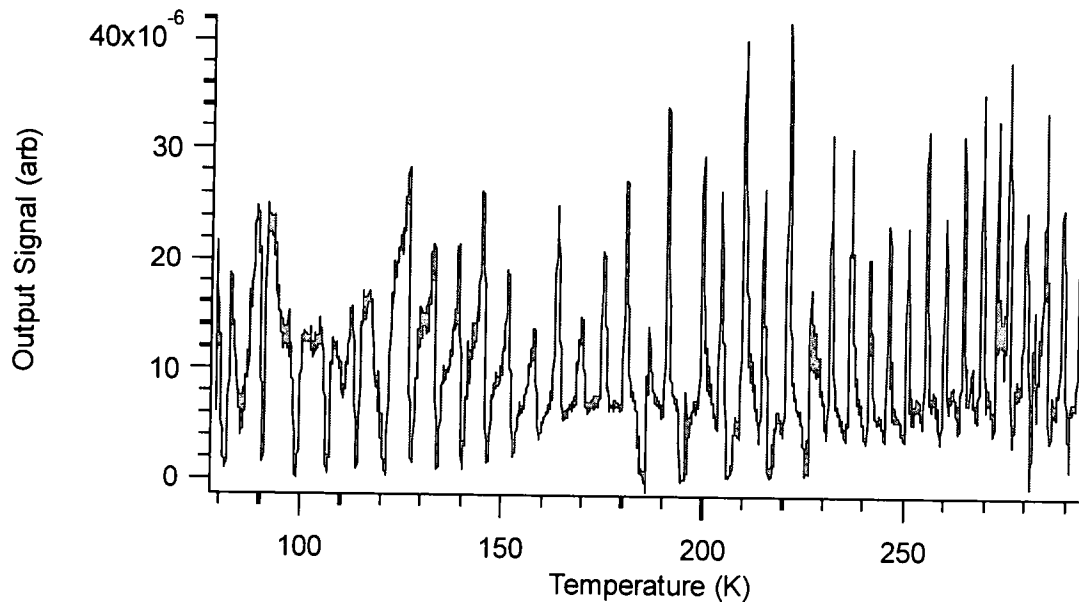


Figure 4.2: Output signal vs. temperature for Ge using Michelson interferometer.

4.1.2 Fabry-Perot Interferometer using Michelson Design

Before we assembled the Fabry-Perot interferometer, the Michelson was adjusted to act like a Fabry-Perot. This was done to be sure the contrast of the interfering beams would be large enough to be measured with the available detectors. By blocking the reference arm (the beam path which does not pass through the sample), the sample is used as a double-pass etalon. As the temperature changes, the optical path difference between multiple internal reflection changes and the total transmission of the sample becomes temperature-dependent. The interference pattern is created by using the sample as an etalon and interfering the transmitted beams that pass through the sample during both passes. As seen in Figure 4.3, the output signal of the beam was still strong enough to create clear constructive and destructive peaks. The rapid change in period between peaks also indicates that the Michelson setup was

problematic with alignment. Specifically, previous studies on the effects of temperature on thickness and index indicated that the change in period between peaks was slow.

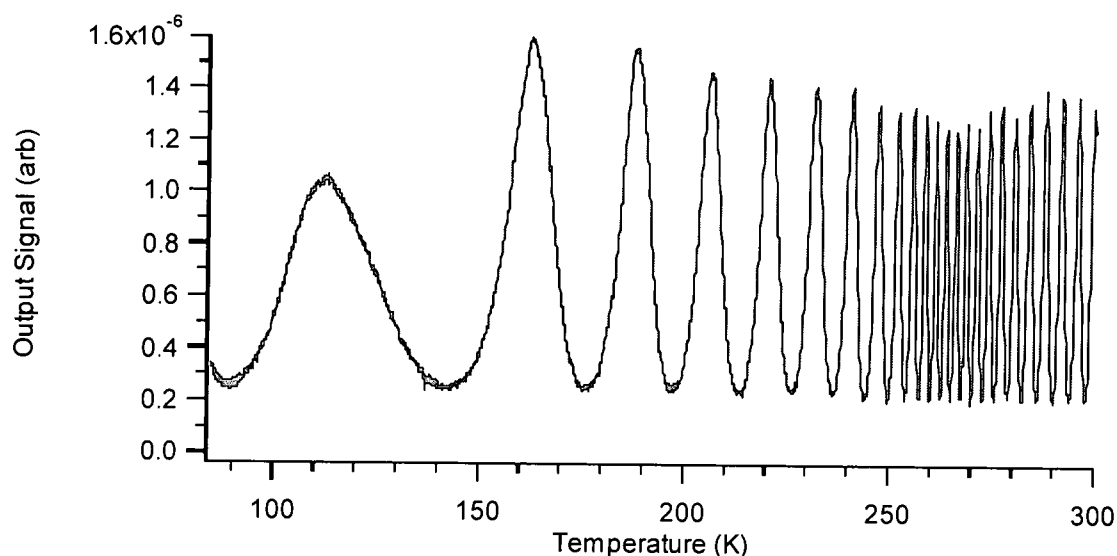


Figure 4.3: Output signal vs. temperature for Ge using Michelson interferometer as Fabry-Perot.

4.1.3 Fabry-Perot Interferometer

A Fabry-Perot interferometer was the final technique used for this aspect of the project. Figure 4.4 shows the general design used for this setup. The lens is placed in the path of the beam to keep the beam from expanding too much and to decrease the spot size through the sample. A large focal length such as 1.5 meters is used to also keep the beam from focusing too fast. This caused the beam to stay a similar size throughout the system. The sample was placed near the beam waist so that in this region the beam was collimated, approximating a plane wave. The two mirrors are used for alignment of the system. The Fabry-Perot resonator is formed by the Fresnel reflections described in Section 3.1. The chopper (ThorLabs MC1000) and pyroelectric detector (Boston Electronics

P.D.-10.6.3) are connected to a lock-in amplifier (Stanford Research Systems SR830 DSP) so the transmitted intensity may be recorded with respect to a set zero value created by the chopper blades. The output of the detector is analyzed the lock-in amplifier. The laser is a wavelength tunable 400mW CO₂ laser tuned to 10.591 μm , a high gain wavelength for this laser.

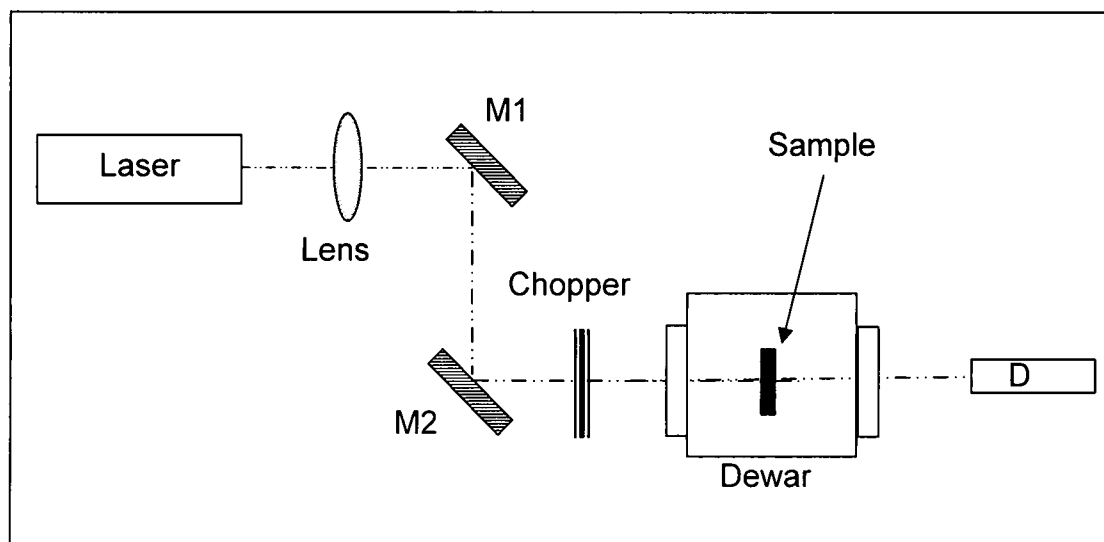


Figure 4.4: Temperature-dependent Fabry-Perot interferometer design.

The sample is held in the temperature controlled dewar (Cryo Industries 110-637-DND) as shown in Figure 4.4. The dewar contains a tank to hold liquid nitrogen for cooling and an integrated heater for heating. It can maintain temperatures between 100-350 K. The dewar windows are AR-coated ZnSe. For infrared wavelengths, these are highly transmissive and therefore don't affect the beam intensity.

To properly record the temperature of the sample, a dewar independent thermocouple is connected to the sample mount. The dewar's integrated thermocouple is not used because it is positioned an inch above the sample next to the heater and nitrogen tank. The distance between the sample and the

thermocouple has two effects: (1) it changes temperature more rapidly than the sample itself can respond to the temperature changes and (2) a temperature gradient exists between the liquid N₂ cell and the sample. Both the difference in thermal response and the absolute temperature were observed experimentally between the integrated thermocouple and the dewar-independent thermocouple.

Thermal paste is placed between the sample, thermocouple, and sample mount. It increases the thermal conductivity between the three and helps the sample and thermocouple maintain the same temperature as the rest of the dewar. Also, it provides flexibility for the sample to expand and contract with temperature while minimizing thermal stress on the sample itself. Every thermal paste is built for a temperature range in which it does not melt or harden. It was decided that to be safe, the Apiezon brand low temperature thermal paste (N) would be used for the collection of data below 300 K. A second high temperature Apiezon brand thermal paste (H) was used for temperatures above 300 K.

The output signal versus temperature data collected using this setup was far clearer than the Michelson interferometer. The overall amplitude changes were also much less than for the data taken with the single arm Michelson setup. Figure 4.5 is a plot of output signal versus temperature using this new setup.

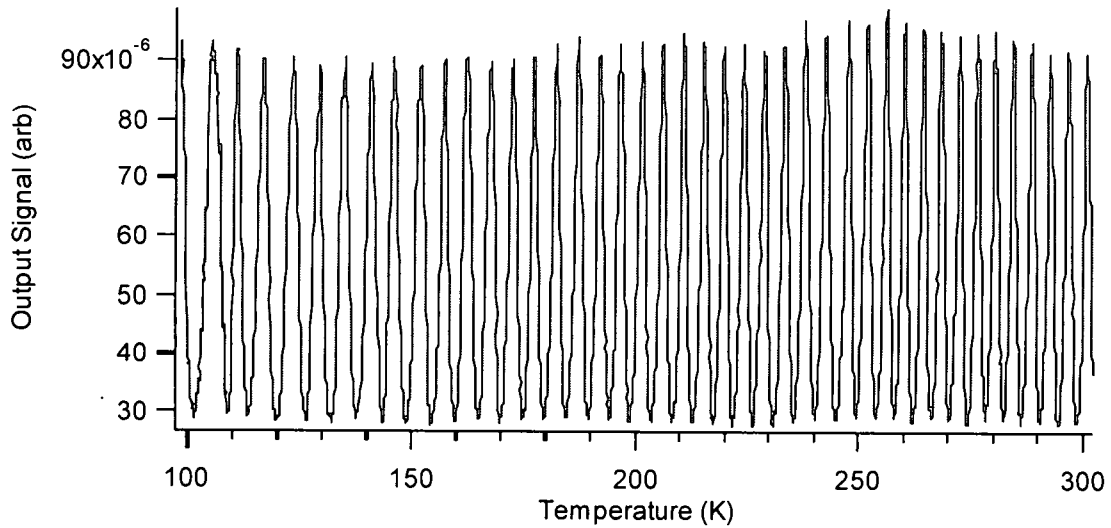


Figure 4.5: Output signal vs. temperature for Ge using Fabry-Perot interferometer.

Using the theory described in Section 3.1, a temperature dependent nL can be calculated as seen in Figure 4.6. As previously mentioned, this experiment provides no information about the absolute value of nL at any location. Hence, the lowest point in Figure 4.6 is set to zero at present.

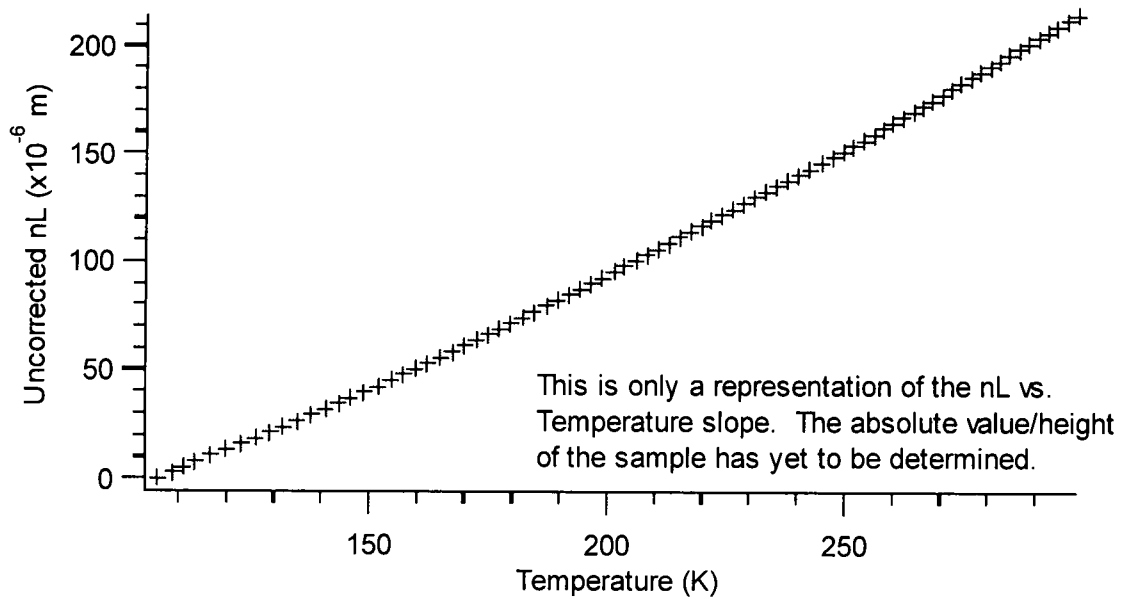


Figure 4.6: Uncorrected nL vs. temperature for Ge using Fabry-Perot interferometer.

4.2 Testing System Accuracy

To test whether or not the system was accurate, the collected nL versus temperature data had to be compared with data collected in previously published works. During the early stages of this project, all data was taken with germanium. This is a very common material which has been well documented and studied in the past. A plot of nL versus temperature was created using the widely used Sellmeier equations from Barnes and Piltch¹⁶, the raw data used to create the Sellmeier equation¹⁷, and a compilation of thickness measurements at different temperatures resulting in a thickness versus temperature equation for Ge¹⁸. Since neither of the absolute value experiments had been created at this early stage in the project, all experimental data was assumed to have the same optical path length at room temperature.

The nL versus temperature plot using the temperature-dependent Fabry-Perot interferometer compared perfectly to the previously recorded data from Icenogle, Platt, and Wolfe¹⁷. Figure 4.7 shows the nL versus temperature plots using two sets of data mentioned and a plot using the Barnes and Piltch Sellmeier equation¹⁶ as a source for the index.

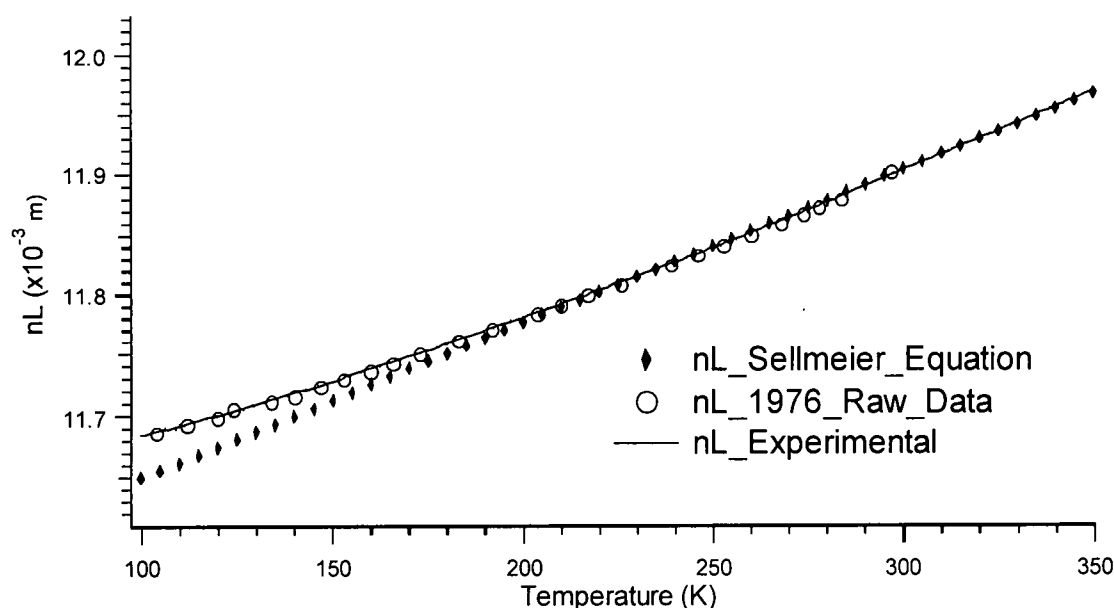


Figure 4.7: nL vs. temperature compared to two other studies.

From Figure 4.7 it is clear that the Ge Sellmeier equation notably deviates for temperatures below 200 K. The Ge Sellmeier equation has been commonly used for the index of refraction since its publication in 1979. The problem with it is that it was modeled using data from three temperatures¹⁶. These were 204 K, 275 K, and 297 K. Hence, it does not accurately depict index values below 204 K. While the original paper itself does not claim to be valid below this temperature, many newer publications consider this equation to be valid between 100 and 295 K¹⁹. The miscommunication was probably due to two problems. First, being a Sellmeier, the equation primarily focuses on the effect of wavelength not temperature. The effect of temperature is negligible when dealing with large wavelength changes. Secondly, while only three temperatures were used in the creation of this Sellmeier equation, the data in which these three temperatures were taken was collected across the range, 100-300 K¹⁷.

Chapter 5

Absolute Value of the Index of Refraction

5.1 *Room Temperature Index of Refraction Measurement*

As mentioned in Chapter 3, the absolute value of the optical path length is needed for at least one temperature to establish the absolute value of the nL versus temperature plot. The simplest temperature to work with is room temperature. Measuring the thickness at room temperature is a simple task and will be discussed further in the next chapter. The index of refraction is not as easily measured. The solution to this problem is an angle-dependent Michelson/Fabry-Perot interferometer. This is a Michelson interferometer in which the angle of the sample is the only variable that affects the path difference between the two arms. It is called a "Michelson/Fabry-Perot interferometer" because data can be taken as a traditional Michelson interferometer, or with the reference arm blocked so that it functions as a Fabry-Perot interferometer (with the sample acting as the etalon).

As mentioned in Section 3.2, collecting data with both setups provides two equations for the two unknowns; thickness and index of refraction. It should be

noted that while the thickness is not necessarily an unknown, collecting the data this way provides a check on the absolute thickness measurement as well. Also, since the sample is probably not perfectly flat parallel, the sample thickness measured in one data run may not be the same thickness measured in another.

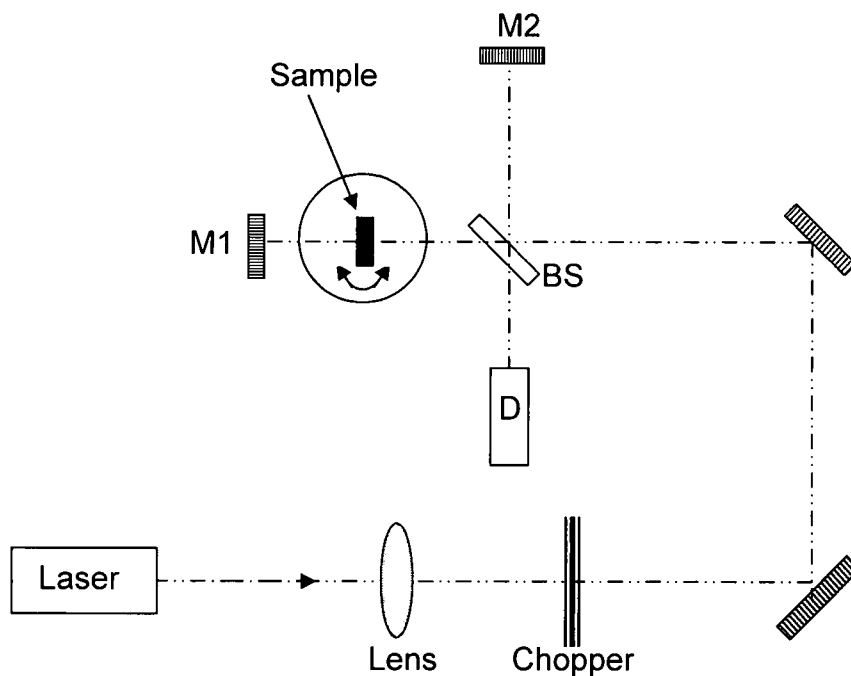


Figure 5.1: Design for Michelson/Fabry-Perot interferometer.

Before the beginning of this project, the angle-dependent Michelson/Fabry-Perot was the experiment used for index measurements in this laboratory^{1,2}. For that reason, it was an easy and obvious addition to the project. Figure 5.1 shows the design used for the interferometer. The focal length of the lens in the system is long such that it has a large Rayleigh range. The optimal location for focus is at the sample mirror, M1 above. This minimizes the size of the beam and therefore maximizes the intensity as it passes through the sample both times. Focusing elsewhere might increase the intensity in the first pass but decrease the intensity in the second pass. The sample is rotated using a rotation

stage which is controlled with an ESP300 Newport Universal Motion Controller. The intensity of the beam is measured using a pyroelectric detector (Boston Electronics P.D.-10.6.3) with the zero value for intensity collected using a lock-in amplifier (Stanford Research Systems SR830 DSP) and a chopper (ThorLabs MC-1000). The same CO₂ laser used for the temperature-dependent Fabry-Perot interferometer is used for this system.

5.2 *Experimental Method*

Measuring the room temperature index of refraction is fairly simple using this method. Once the Michelson interferometer is setup and aligned, the sample wafer is placed in the system. It is important to have the sample aligned such that the incident beam passes through the sample in the axis of rotation. If this is not the case, the data will be skewed and inaccurate.

With the sample aligned, the sample angle must be measured. The easiest way to do this is to find the angle of normal incidence. At normal incidence, the reflected component of the laser on the sample will pass into the detector and cause a notable peak. Figures 5.2 and 5.3 in this chapter provide good examples of back reflection from normal incidence on the sample.

Data collection consists of ten measurements with the Michelson and Fabry-Perot setups collected without any changes to the system. Specifically, no changes may be made during any set of data, one Michelson and one Fabry-Perot recording, since the data from the two will be combined using the above theory. Changes between sets of data would be acceptable (though unneeded). An example of an acceptable change to the system is the case where the system

is knocked out of alignment in some way and has to be fixed. Each set of data is collected across as large an angular range as possible. This is simply because larger angular ranges yield more data to work with which reduces the amount of uncertainty in the measured values. Generally, the sample is rotated a total of 40-50 degrees centered at normal incidence. After 25 degrees rotation in either direction, the output signal of the Fabry-Perot decreases too much to be usable. Figures 5.2 and 5.3 depict the output signal versus angle for Michelson and Fabry-Perot setups, respectively, using InAs. The angle dependent Michelson/Fabry-Perot was tested using InAs and later checked with Ge and Si.

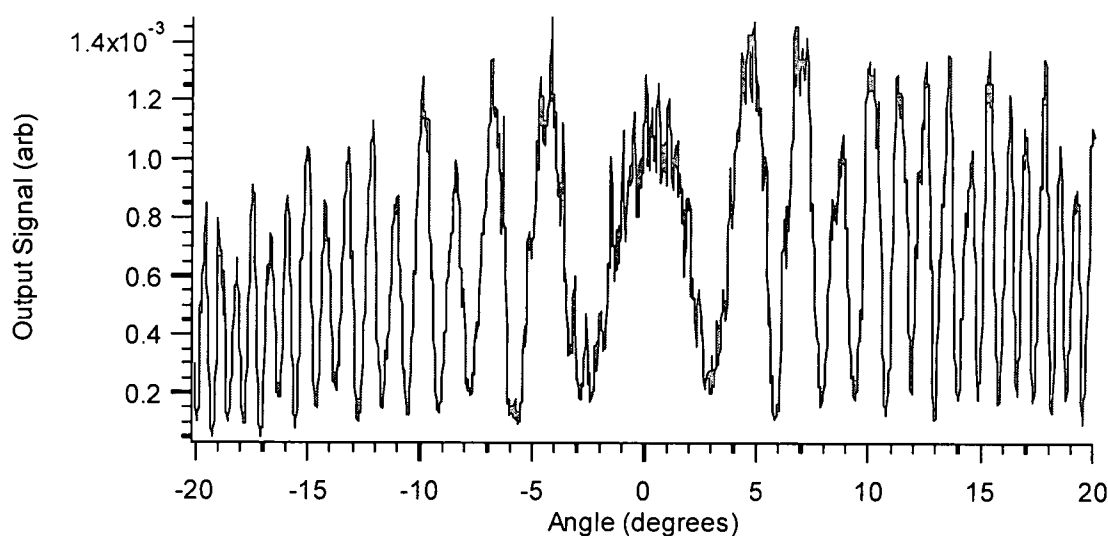


Figure 5.2: Output signal vs. angle for Michelson interferometer using InAs.

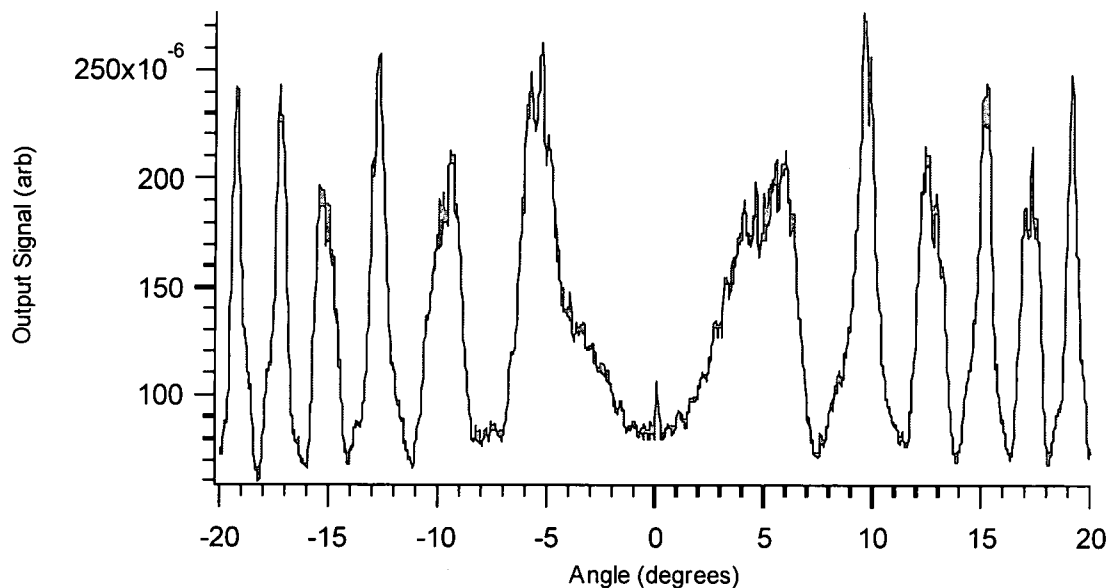


Figure 5.3: Output signal vs. angle for Fabry-Perot interferometer using InAs.

Similar to the temperature-dependent Fabry-Perot interferometer, the angle dependent phase change is created using the constructive and destructive peaks. In this case, a program is used to set an average height across the above plots. It then fits a sine wave to the space between every two points that intersect the horizontal line. This is just a more accurate way to evaluate the locations of the peaks and valleys in the data in comparison to general estimates. The program ignores a given angular range in the center of the plot, for example -5 to 5 degrees, because this data is affected by back reflection off the sample surface. Using the locations of the constructive and destructive peaks, a phase versus angle plot can be created for both the Michelson and Fabry-Perot data. These plots are depicted below in Figures 5.4 and 5.5. The Fabry-Perot phase change is negative because the phase is a decreasing function with respect to increasing angular orientations, as seen in Equation (3.8). Generally, the program used for creating the phase versus angle plots is accurate. In cases

where the data is too weak or noisy though, the program also contains a manual control which allows the “average” value to be chosen.

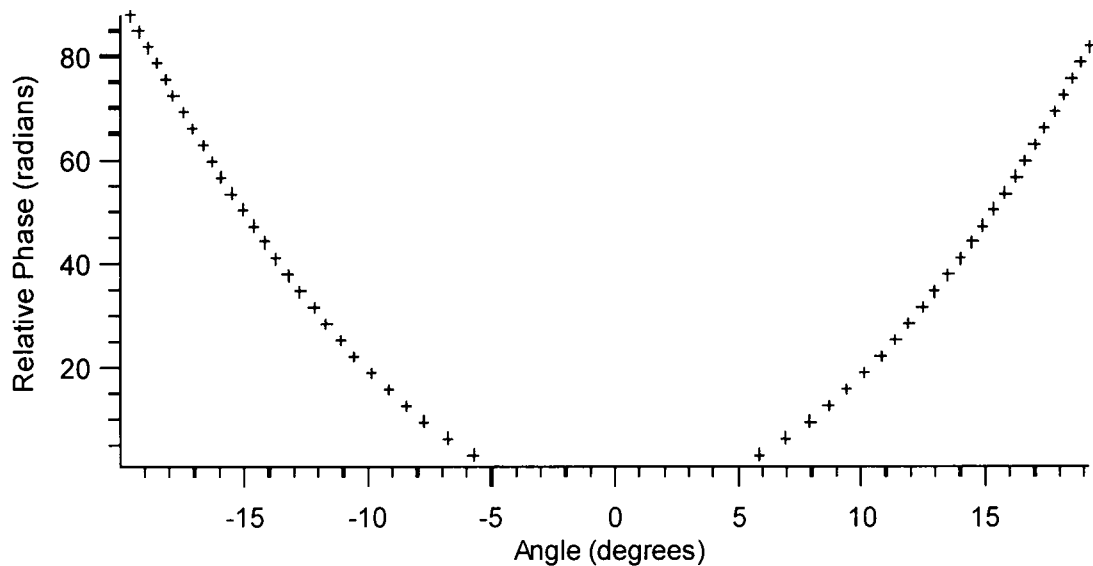


Figure 5.4: Phase vs. angle for Michelson interferometer using InAs.

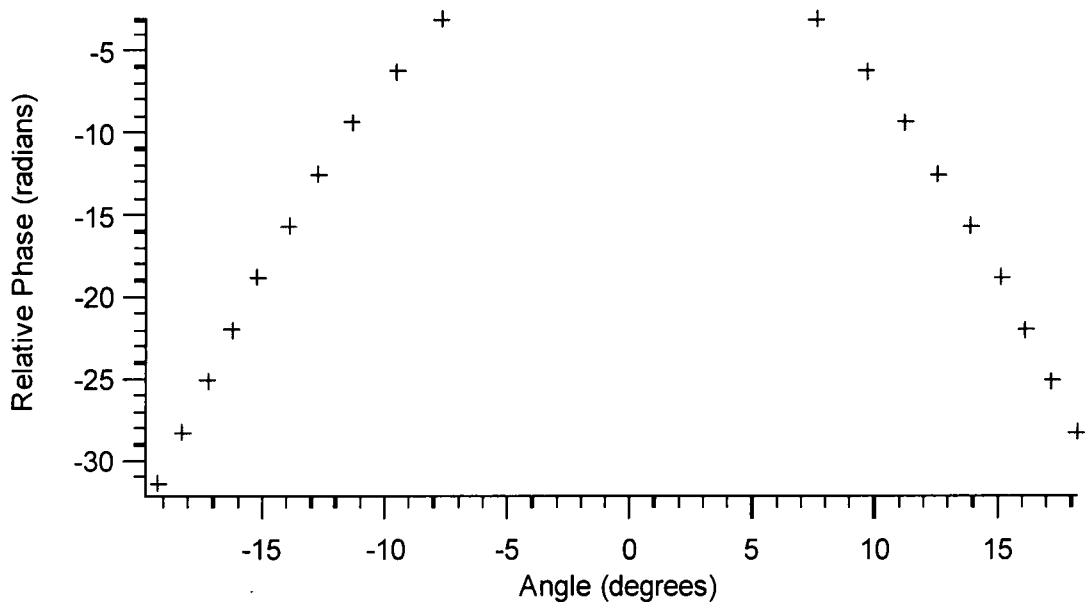


Figure 5.5: Phase vs. angle for Fabry-Perot interferometer using InAs.

Once the phase versus angle plots are created, a final program is used to fit a curve to each and then subtract the Fabry-Perot from the Michelson data as seen in Figure 5.6. The phase difference versus angle plot is then used to

discern the thickness and index of refraction values using Equations (3.10) and (3.8) or (3.9).

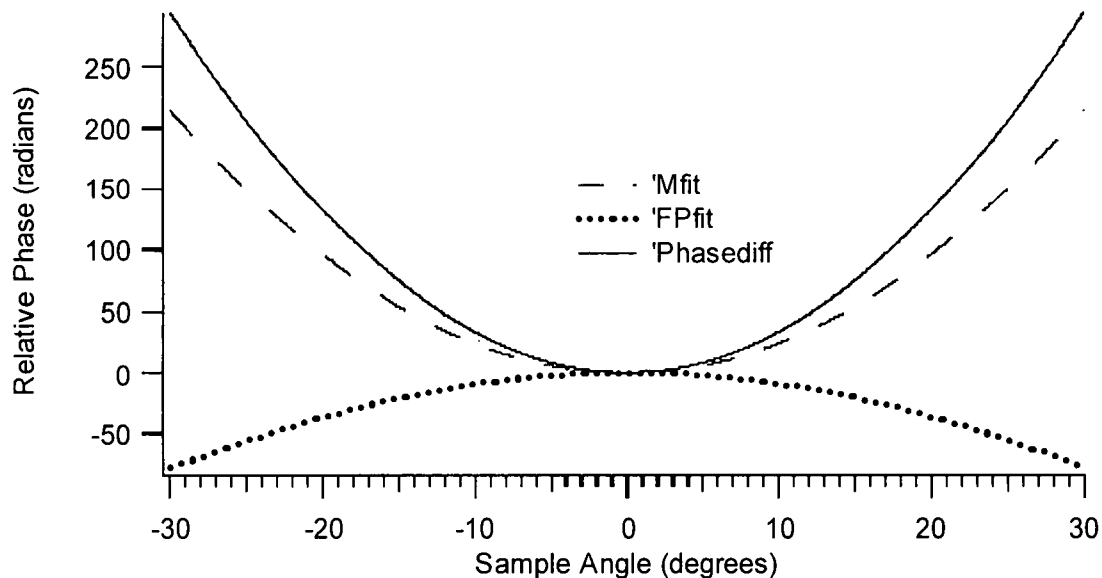


Figure 5.6: Phase difference and Michelson and Fabry-Perot phases vs. angle using InAs.

5.3 Cryogenic Temperature Index of Refraction Measurement

Originally, when well documented materials such as germanium were being studied, only one absolute value was needed. This was because it was known that the index of refraction decreased with temperature. While this is true for most elements and compounds, it is not always true. The sign of the change of n with respect to temperature is also not known from the temperature dependent Fabry-Perot interferometer because that only indicates the magnitude of the change in the optical path length. Whether or not the change is positive or negative is unknown.

For this reason, a second angle-dependent Michelson/Fabry-Perot was built in which the sample was kept inside a temperature controlled dewar as seen

in Figure 5.7. The only reason both setups were built was that the need for two temperatures was not realized until after the temperature independent experiment had been built. The second setup is usable for both measurements, making the first obsolete for further experiments. Also, unlike the commercial dewar in the temperature-dependent Fabry-Perot from the last chapter, this dewar is home-built and has no heater and therefore is only useful for room and cryogenic temperatures. The setup for this system is identical to the room temperature version except for the dewar which now contains a vacuum-sealed rotation feed through which the sample can be rotated within a stationary housing.

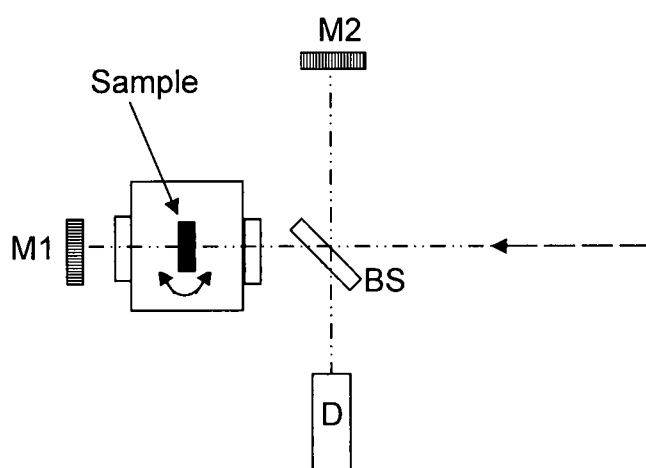


Figure 5.7: Temperature and angle-dependent Michelson/Fabry-Perot interferometer.

Chapter 6

Thermal Expansion Coefficient and Absolute Thickness Measurements

6.1 *LaserMike Optical Micrometer*

The LaserMike optical micrometer is a thickness measuring device. The device contains a HeNe laser which is spanned out into a scanning planar output. The laser plane then passes across an area where a sample may be placed. The sample blocks some of the plane leaving a shadow. The HeNe is then collected on the other side of the sample area and the thickness of the sample is calculated using the size of the shadow cast. By scanning the laser across the sample and observing the transmitted light signal, the LaserMike converts a physical thickness measurement into a time measurement, which can be very accurate. This device, when calibrated is accurate to $\pm 0.127 \mu\text{m}$ and therefore the best source of absolute thickness measurements for any samples used.

6.2 *Absolute Thickness Measurements*

Many measurements are required for measuring the thickness of a sample. If the sample were perfectly flat parallel, then only one measurement

would be needed. Unfortunately, few samples are ever perfectly designed so an array of alignments must be made to fully document a sample's thickness.

The first step in taking thickness measurements is to add an adjustable table to the system. The sample is then placed on the table. This table allows the sample to lay at the height needed to intercept the beam path. The table also contains an adjustable slit down the middle such that the beam is only affected by the sample. Finally, the table has an adjustable tilt controlled by two knobs much like an adjustable mirror. This allows the sample to be tilted slightly to find the minimum thickness of the sample across any plane. Figure 6.1 shows a general exterior design of the LaserMike optical micrometer when setup to measure the absolute thickness at room temperature.

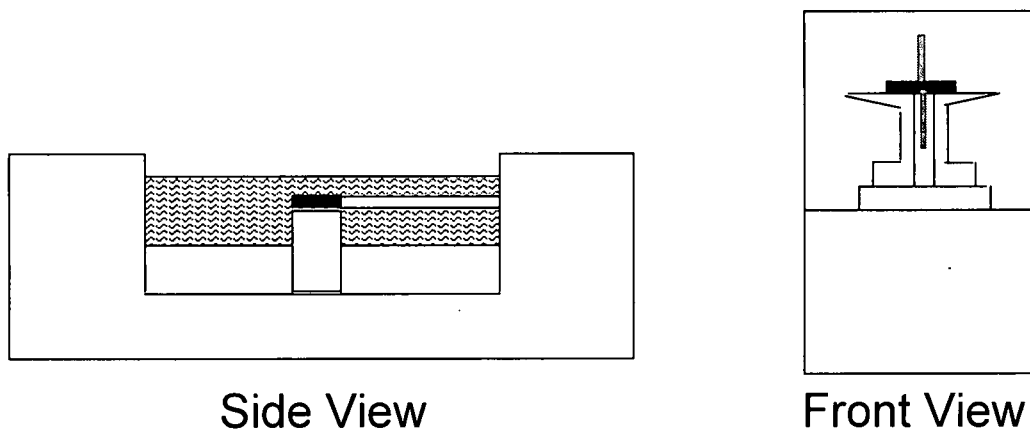


Figure 6.1: LaserMike optical Micrometer Setup for Room Temperature Measurements.

Once the table is aligned and the sample is placed in the path of the beam it is time to take measurements. The first set of measurements is used to discern the minimum thickness through the center of the sample (or whatever location on the sample that the laser will pass through) in the interferometric experiments. This is done by placing the center of the sample in the beam plane. After

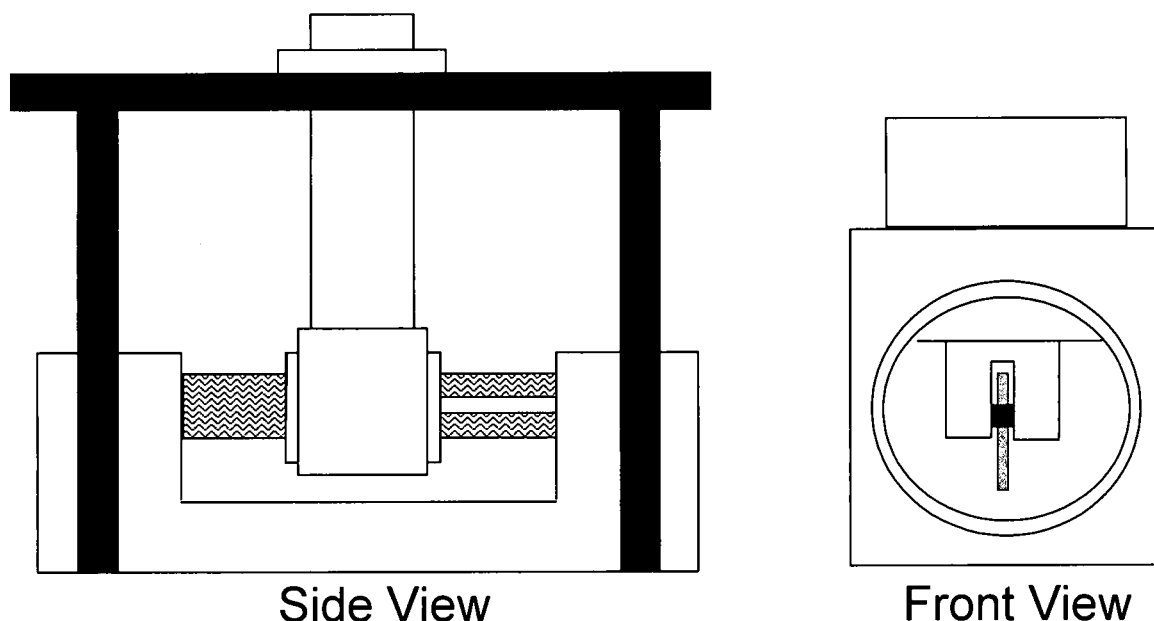


Figure 6.2: LaserMike optical Micrometer Design for Room and Cryogenic Temperature Measurements.

The first important issue was the sample mount. The new mount seen in the front view in Figure 6.2 was built for just this experiment. It is a cup shaped holder in which the sample may be placed flat along its bottom. A slit is carved through the mount such that it does not affect the path of the beam. The mount may then be attached the dewar. The dewar independent thermocouple used in the temperature-dependent Fabry-Perot interferometer attaches to the bottom of the new mount. No thermal paste is used between the sample and the mount. During testing of the system, it was determined that the thermal paste caused the sample to change positions as the paste itself expands or contracts with temperature.

The second issue was the effect of vibration. Originally, the dewar housing was placed on a pedestal so that is was kept at the right height for the beam path. The problem with this was that the sample is mechanically coupled to the internal portion of the dewar. The internal portion of the dewar lay atop the

dewar housing with an o-ring placed in between to hold the interior in vacuum. The o-ring connection between the two dewar pieces can allow one to move or vibrate with respect to the other. For the accuracy of these measurements, it was decided that mechanically coupling the dewar housing to the LaserMike would still allow vibrations to change the position of the sample during measurements. To alleviate this problem, a new dewar mount was built such that the portion of the dewar directly connected to the sample was held solid at all times. This mount suspended the dewar in the air as seen in the side view in Figure 2.

The final issue with this system was the effect of back reflection from the dewar windows. For the LaserMike to work, the HeNe must not reflect back into itself. This causes major errors in the system. Normally, this would be solved with AR coated windows and tilting the dewar slightly off normal incidence. Unfortunately, the dewar windows had to be near normal incidence so that temperature changes do not affect the angle of refraction through the windows and therefore cause the beam to measure across different cross-sections of the sample. Also, there were no available AR coated windows in the lab for a HeNe wavelength, 632.8 nm. To minimize this error, the ZnSe windows were switched to CaF_2 , a highly transmissive material for red light. The dewar was then tilted very slightly off normal incidence. The angle of change was very negligible so a beam block had to be placed alongside the output of the beam. The dewar was adjusted such that the block did not affect the HeNe output but did block the reflection off the dewar window.

The combination of all these specific setup details allows for accurate measurements of the thickness to be taken at both room and cryogenic temperatures. Temperatures between room and cryogenic were not measured because the dewar can maintain only these two temperatures for an extended period. Due to the lack of thermal paste between sample and mount, this extended period of time is needed to be certain the sample and thermocouple are kept at the same temperature.

Using this design, a linear thermal expansion coefficient can be measured using the theory derived in Section 3.3. Once α has been accurately measured, the thickness at room temperature can be measured using the absolute thickness and temperature readings taken in section 5.2. The measurements taken with the dewar can not be used for an absolute number because the sample is not adjusted to minimize the shadow cast in the LaserMike, which can result in a larger than actual measurement. The thermal expansion coefficient is the same across any cross-section of a uniform material. The material may even be on edge such that the temperature's effect on height, width, and length affect the thickness measurements. This is why the coefficient may be measured in one setup and then used for another. We are also assuming the thermal expansion coefficient is uniform in all directions, which is a good assumption for semiconductors which have cubic structures.

Chapter 7

Results

Using the data collected from all three experiments, the temperature-dependent index of refraction and thermo-optic coefficient can be calculated. Presently, these values have been measured for four samples. Germanium and Silicon were measured to show that the techniques used were accurate and reproducible since these values have been well documented for both materials by previous publications¹⁷. The temperature dependent refractive index and thermo-optic coefficients of indium arsenide and indium antimonide were then measured. To the best of our knowledge, neither of these materials has had these values previously published. In both cases though, the index of refraction at room temperature and a linear thermal expansion coefficient had been previously published.

For the case of indium antimonide, data was collected from 100-200 K. This was because the transmission of InSb is dependent on temperature. At 10.591 μm , the transmission is approximately 90% between 77-175 K. It then decreases rapidly as the temperature increases. This is due to the small

bandgap in InSb where at room temperature significant numbers of carriers are thermally excited. Due to such a drastic change, the temperature-dependent Fabry-Perot interferometer could not be used to provide an optical path length versus temperature plot above approximately 200K.

7.1 *Angle Dependent Michelson/Fabry Interferometer Data*

Two sets of data were collected using both Ge and Si to test the accuracy of the angle-dependent Michelson/Fabry-Perot interferometer. Table 7.1 compares this data with the absolute thickness measurements from the LaserMike optical micrometer and published index of refraction measurements at room temperature. More trials may have been completed if not for the fact that this aspect of the project was already built and used for previous publications on these very materials^{1,2}. The index of refraction at cryogenic temperatures were not measured in this study for germanium and silicon because these measurements had previously been made using this setup and method^{1,2}.

Table 7.1: Index and thickness measurements for Ge and Si using Michelson/Fabry-Perot.

Trial	Ge (296 K)		Si (296 K)	
	n	L (m)	n	L (m)
1	3.9945	0.0029705	3.4058	0.0029836
2	4.0023	0.0029637	3.4097	0.0029838
Average	3.9984	0.0029671	3.40775	.0029837
Expected	4.0 [20]	0.0029710	3.42 [20]	.0029781

With the system properly aligned and tested, index measurements were taken for indium antimonide and indium arsenide for room and cryogenic temperatures as seen in Tables 7.2 and 7.3. In the case of indium antimonide, room temperature data could not be taken due to the weak transmission.

Similarly, accurate cryogenic temperature data could not be collected for the Fabry-Perot design since proper alignment changes could not be made at room temperature. For this reason, only a Michelson design was used for Indium antimonide at cryogenic temperature. The refractive index was measured by considering the thickness to be a constant dictated by the LaserMike optical micrometer measurements. The sign of the temperature dependence on the refractive index was found by comparing known values of InSb at room temperature (3.94 at 300K²⁰) and comparing them to the newly measured value at cryogenic.

Table 7.2: Index and thickness measurements for InAs using Michelson/Fabry-Perot.

Trial	InAs (294 K)		InAs (102.15 K)	
	n	L (m)	n	L (m)
1	3.4787	0.0018623	3.4190	0.0018476
2	3.4919	0.0018589	3.4291	0.0018528
3	3.4781	0.0018537	3.4283	0.0018546
4	3.4975	0.0018507	3.4430	0.0018520
5	3.4853	0.0018568	3.4285	0.0018554
6	3.4905	0.0018541	--	--
7	3.5253	0.0018462	--	--
8	3.4603	0.0018589	--	--
9	3.4885	0.0018508	--	--
10	3.4712	0.0018532	--	--
Average	3.485 ± .009	0.001855 ± 4E-6	3.430 ± .009	0.001852 ± 3E-6
Expected	3.51 [20]	0.0018459	---	0.0018448

Table 7.3: Index and thickness measurements for InSb using Michelson/Fabry-Perot.

Trial	InSb (95.85 K)	
	n	L (m)
1	3.8346	0.0020992
2	3.8664	0.0020992
3	3.7542	0.0020992
4	3.8372	0.0020992
5	3.9143	0.0020992
6	3.8230	0.0020992
7	3.7740	0.0020992
8	3.8983	0.0020992
9	3.7323	0.0020992
Average	3.83 ± 0.06	0.0020992 ± 0
Expected	----	-----

7.2 LaserMike Optical Micrometer Data

For each material studied, two to three sets of data were taken at room and cryogenic temperature to measure the value of the linear thermal expansion coefficient. As mentioned in Section 5.3, these were the only two temperatures that could be measured accurately due to the system design. Table 7.4 contains the data for each trial and the consequent calculated average α values using Equation (3.12).

Table 7.4: Linear thermal expansion coefficient data.

Trial	T_2 (K)	$L(T_2)$ (mm)	T_1 (K)	$L(T_1)$ (mm)	α ($10^{-6}K^{-1}$)
Ge 1	349.7	2.9774	349.7	2.9781	6.262
Ge 2	296.5	2.9774	103.8	2.9743	5.333
Si 1	299.8	2.9850	99.4	2.9841	1.505
Si 2	299.8	2.9870	99.9	2.9844	4.438
InAs 1	297.9	1.8410	113.2	1.8382	8.235
InAs 2	296.4	1.8395	112.5	1.8367	8.277
InSb 1	298.1	2.1097	113.0	2.1062	8.456
InSb 2	297.2	2.0195	115.0	2.1057	9.913
InSb 3	297.6	2.1090	113.5	2.1062	7.196

Averaging the values of the linear thermal expansion coefficients from Table 7.4 provides a final value for this coefficient. Table 7.5 lists the final linear

thermal expansion coefficients, previously published linear thermal expansion coefficients and the error between them. It is clear from the results that this experiment is the region of largest error in this project. This is acceptable though because the change in thickness is approximately an order of magnitude smaller than the change in index with temperature. The thickness could be held constant with temperature and the index measurements would still be reasonably accurate. Measuring a general linear thermal expansion coefficient just decreases the already small error in the index measurements caused by thickness changes. It should also be noted that there is a lot of variation in previous measurements of α as well. The two referenced InSb values of α are different by approximately 30%^{20,21}.

Table 7.5: Accuracy of linear thermal expansion calculations.

Material	α experimental (10^{-6}K^{-1})	α Published at 300 K (10^{-6}K^{-1})	Error (%)
Ge	5.798	5.9 [20]	1.7
Si	2.971	2.6 [20]	14.3
InAs	8.256	4.52 [20]	82.7
		5.238 [21]	57.6
InSb	8.522	5.37 [20]	58.7
		7.017 [21]	21.44

The thermal expansion coefficient and the absolute thickness measurements at 298 K made with the LaserMike can then be used to create a full temperature dependent thickness equation. Table 7.6 provides the full temperature dependent thickness equations for each material.

Table 7.6: Temperature dependent thickness equations.

Material	$L(T)$
Ge	$2.9678(1 + 5.798 \cdot 10^{-6}(T - 298))$
Si	$2.9780(1 + 2.971 \cdot 10^{-6}(T - 298))$
InAs	$1.8460(1 + 8.256 \cdot 10^{-6}(T - 298))$
InSb	$2.1029(1 + 8.522 \cdot 10^{-6}(T - 298))$

7.3 Temperature Dependent Fabry-Perot Data

With absolute thickness and index of refraction measurements from the other two experiments, the absolute height of the nL versus temperature plots for each material could be set by increasing the value of every point in an uncorrected plot; i.e. Figure 4.6, by the difference between its present value and the absolute value of nL at the measured temperature. Figures 7.1-7.4 display the corrected temperature dependent nL plots for all studied materials. For each sample, multiple sets of data were collected for both cold temperature scans, 100-300 K, and hot temperature scans, 280-350 K. This data was then compiled to create the following plots.

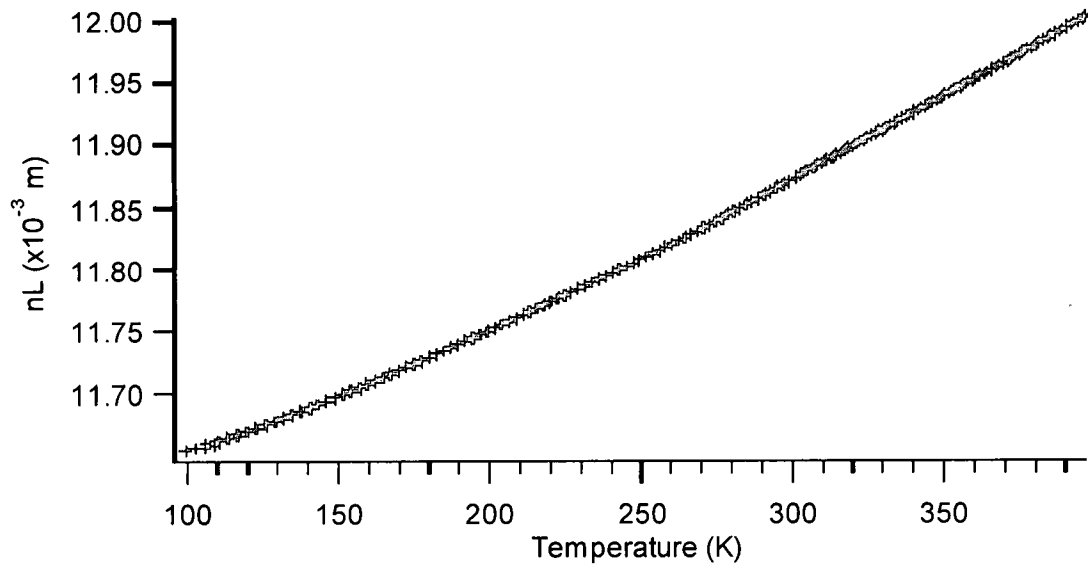


Figure 7.1: nL vs. temperature for Ge.

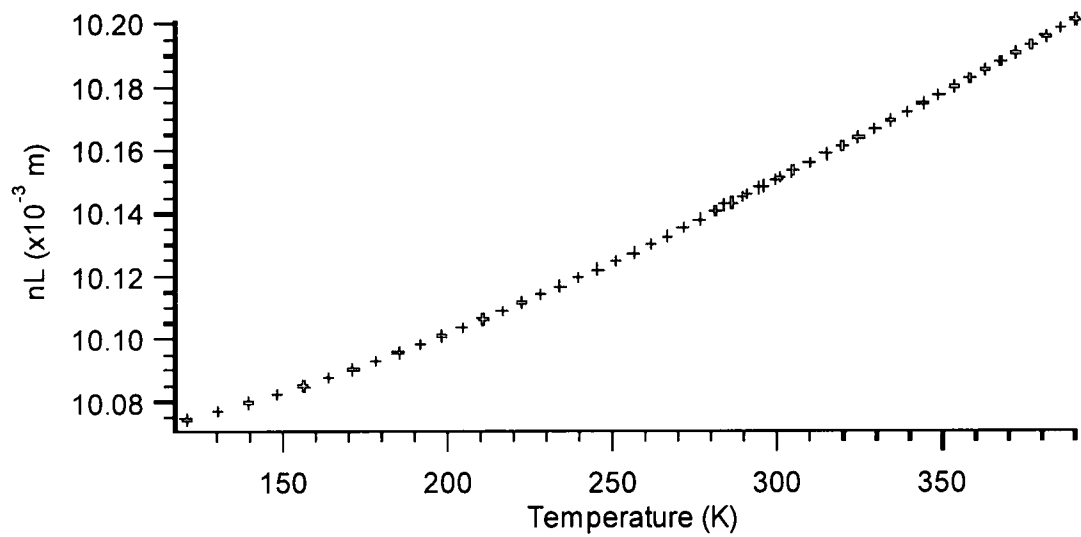


Figure 7.2: nL vs. temperature for Si.

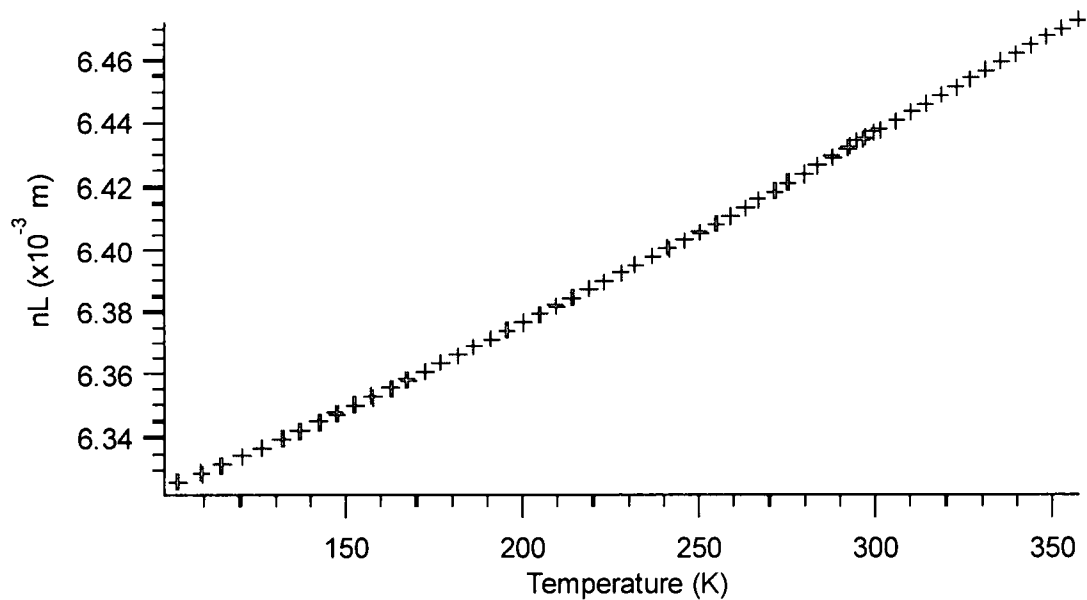


Figure 7.3: nL vs. temperature for InAs

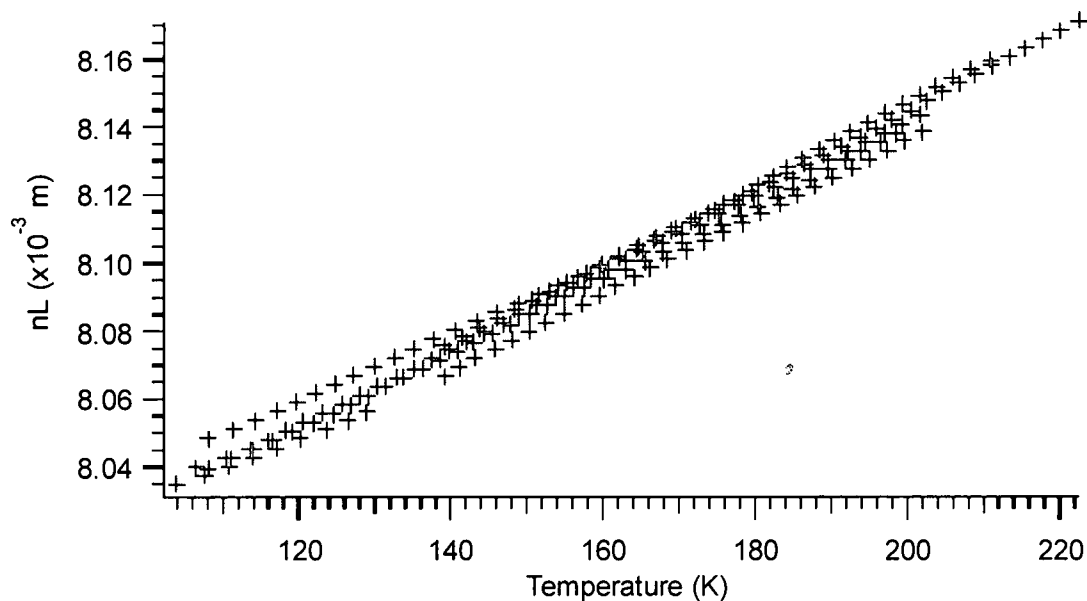


Figure 7.4: nL vs. temperature for InSb

7.4 Final Results and Discussion

To calculate the temperature dependent index of refraction, the temperature dependent optical path length must be divided by the temperature dependent thickness as expressed in Equation (3.13). This is done by dividing

the value of every point in Figures 7.1-7.4 by the thickness for that material and temperature dictated by the temperature functions in Table 7.6. Similarly, the thermo-optic coefficient may be calculated by measuring the slope between any two values of n and setting that as the value of dn/dT at the average temperature of the two points used in the calculation. This calculation is done independently for each set of collected data and then compiled for fitting. Figures 7.5-7.12 are the collected data for the index of refraction and thermo-optic coefficient for all four samples studied. Tables 7.7 and 7.8 provide the coefficients of the polynomial fits for each set of data. Figure 7.13 shows both the calculated dn/dT fit from Table 7.8 and the derivative of the n fit from Table 7.7 for Ge. As expected, they overlap. While the thermo-optic coefficient is simply the derivative of the temperature-dependent refractive index and may easily be measured accurately in this way, the above mentioned calculation was used for the purpose of considering the effect of error in the system on both n and dn/dT . These effects are described in the following paragraphs.

All three experiments were susceptible to many errors. The temperature-dependent Fabry-Perot interferometer error is caused by inaccuracies in temperature readings, problems with system alignment, and assumptions made about how flat-parallel a sample actually is. Similarly, the angle-dependent Michelson/Fabry-Perot interferometer error is caused by the same issues except that it is temperature independent. System alignment is much more important for removing error in this setup. The temperature-dependent optical micrometer was by far the most inaccurate experimental design used in this project. As seen in

Table 7.5, issues such as back-reflection from dewar windows and dependence on the angle of incidence of the HeNe on the dewar windows affected the thickness measurements. Also, due to vibrations and temperature issues in the system, only a linear thermal expansion coefficient could be measured.

While the thermal expansion coefficient measurements contain the greatest error of the three experiments used in this project, it has almost no affect on the overall error in the n and dn/dT measurements because it only represents the error in the almost negligible change in thickness as temperature changes. The errors from the absolute value and slope of nL measurements have a much greater affect on the final measurements since they relate directly to errors in the final calculations. The error in the thermo-optic coefficient calculations is specifically caused by errors or problems in the temperature-dependent Fabry-Perot interferometer. Small errors in the actual location of the constructive and destructive peaks of the output signal versus temperature plot can create a large error in the calculation of dn/dT using the process described above. In addition, since the value of each point in the dn/dT plots is the slope between two specific points in the n versus T data, small point to point errors and fluctuations in the n versus T data results in much larger spreads and point to point variations in the final dn/dT versus T graphs. To decrease this error, more data sets are collected for this aspect of the project than any other.

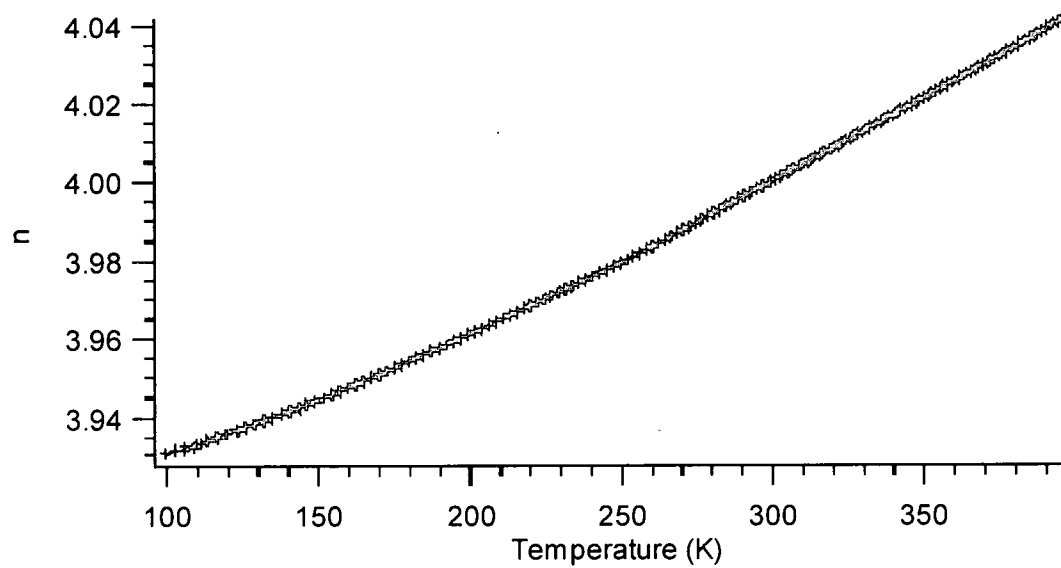


Figure 7.5: n vs. temperature for Ge.

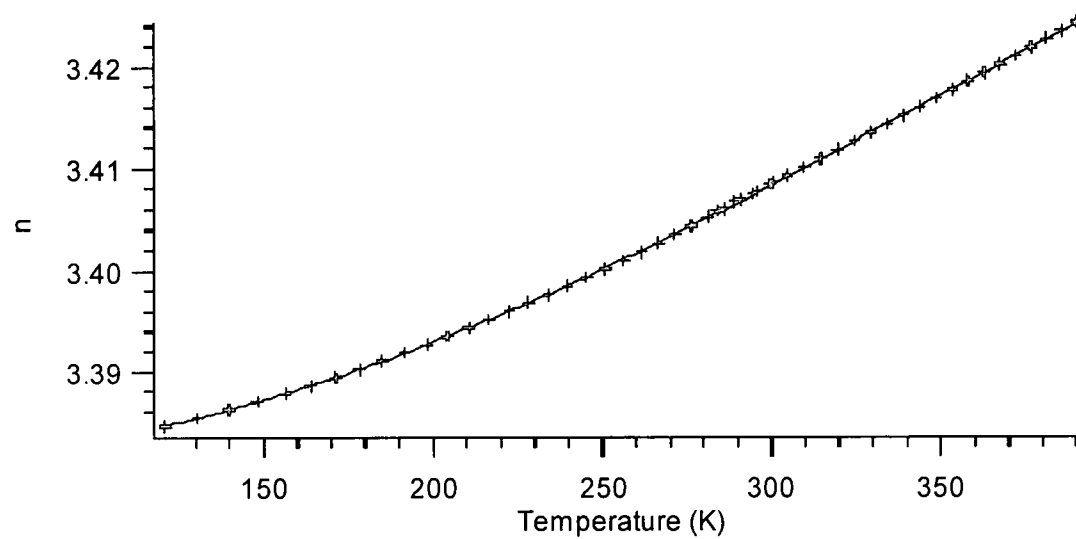


Figure 7.6: n vs. temperature for Si.

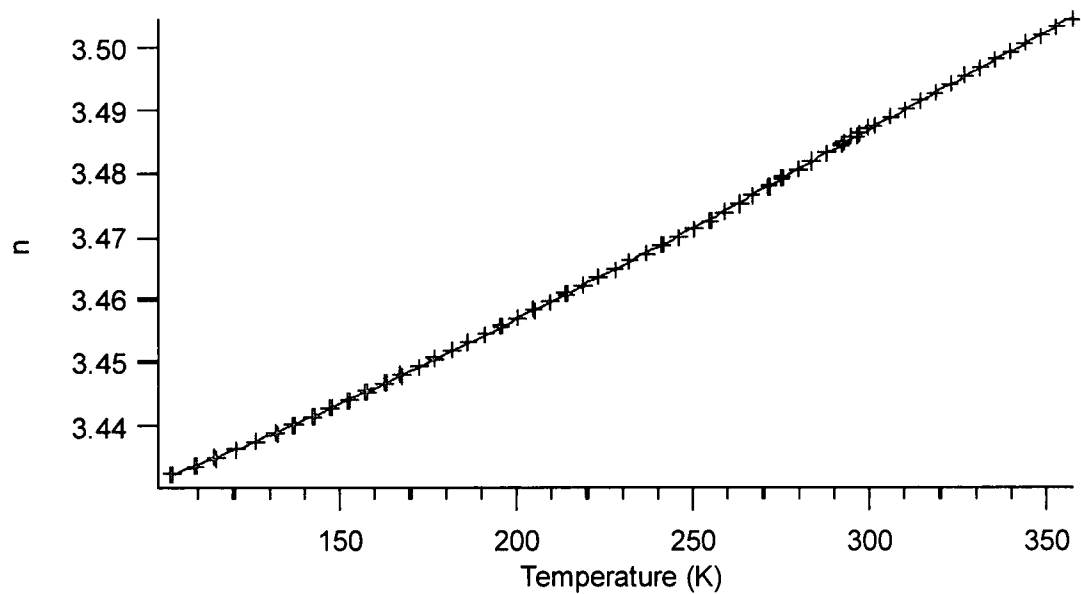


Figure 7.7: n vs. temperature for InAs.

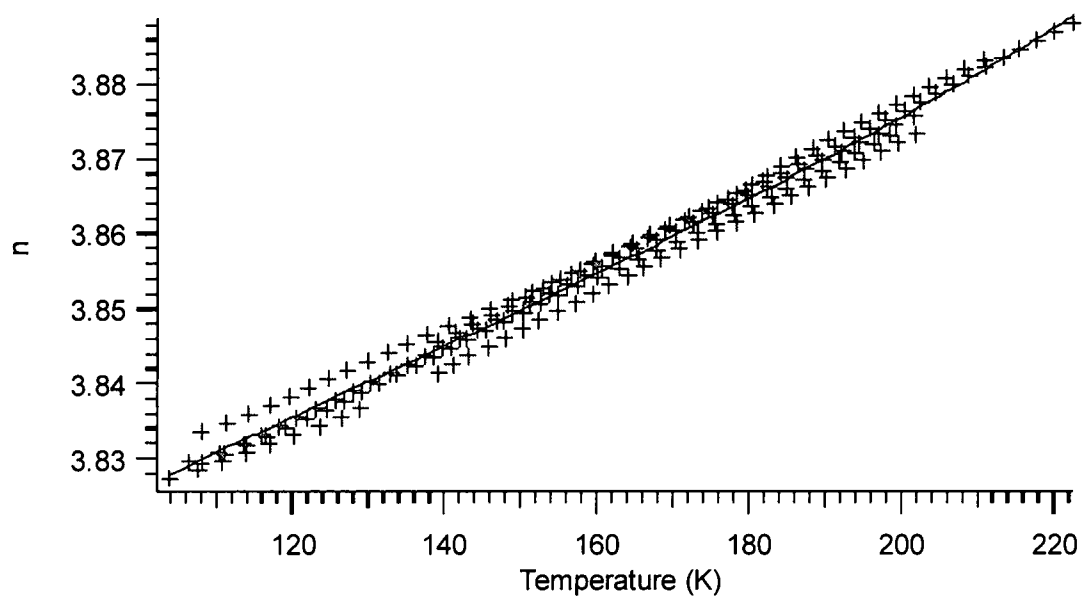


Figure 7.8: n vs. temperature for InSb.

Table 7.7: n vs. temperature function coefficients

Material	$n = A + BT + CT^2 + DT^3$			
	A	B	C	D
Ge	3.9135 ± 0.00031	$9.2077\text{e-}05 \pm 4.14\text{e-}06$	$8.7754\text{e-}07 \pm 1.72\text{e-}08$	$-7.4801\text{e-}10 \pm 2.26\text{e-}11$
Si	3.3825 ± 0.000294	$-5.0112\text{e-}05 \pm 3.74\text{e-}06$	$6.2357\text{e-}07 \pm 1.5\text{e-}08$	$-5.6706\text{e-}10 \pm 1.92\text{e-}11$
InAs	3.4165 ± 0.000507	$9.0409\text{e-}05 \pm 7.4\text{e-}06$	$7.0525\text{e-}07 \pm 3.39\text{e-}08$	$-7.4603\text{e-}10 \pm 4.94\text{e-}11$
InSb	3.7618 ± 0.0183	0.00085209 ± 0.000352	$-2.8328\text{e-}06 \pm 2.22\text{e-}06$	$7.0672\text{e-}09 \pm 4.57\text{e-}09$

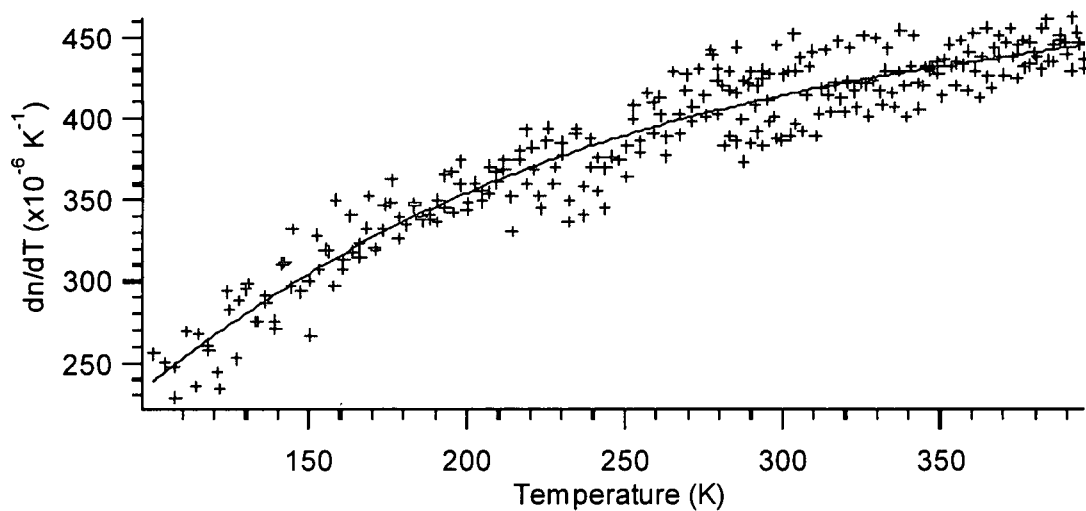


Figure 7.9: dn/dT vs. temperature for Ge.

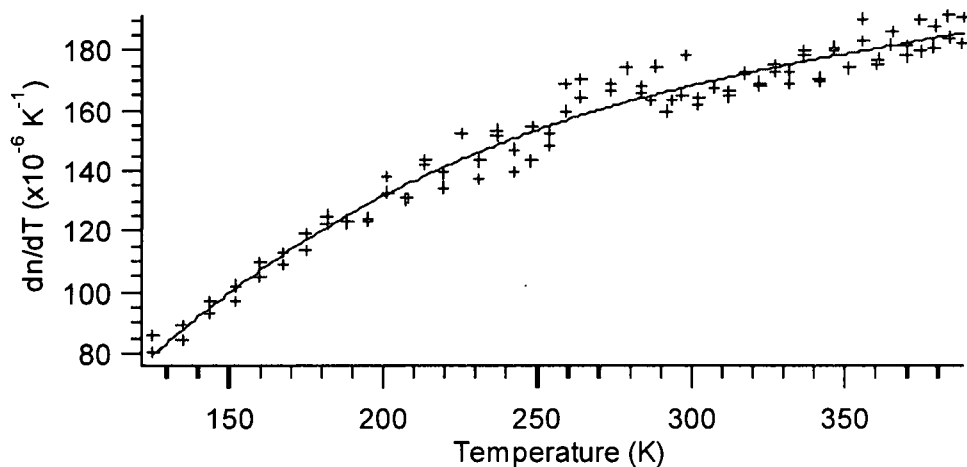


Figure 7.10: dn/dT vs. temperature for Si.

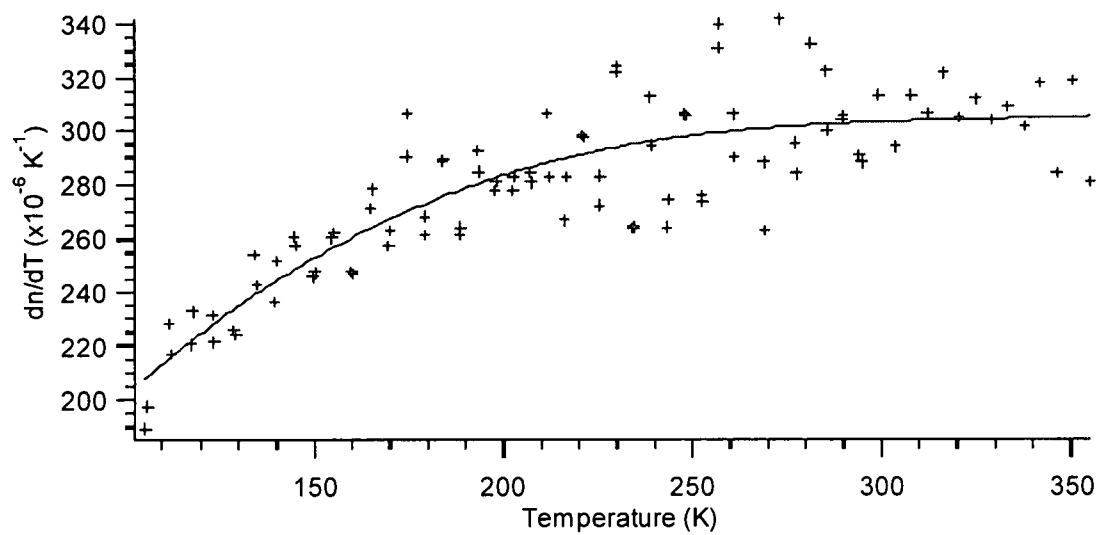


Figure 7.11: dn/dT vs. temperature for InAs.

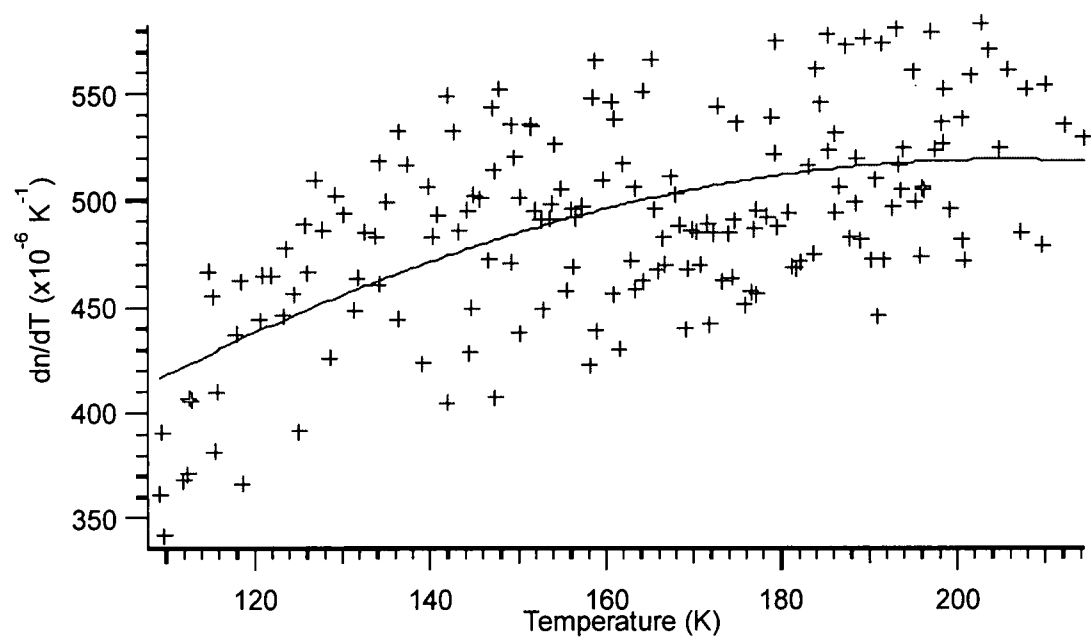


Figure 7.12: dn/dT vs. temperature for InSb.

Table 7.8: dn/dT vs. temperature function coefficients.

Material	$dn/dT = E + FT + GT^2 + HT^3$			
	E	F	G	H
Ge	$2.975e-05 \pm 3.01e-05$	$2.6222e-06 \pm 3.98e-07$	$-6.033e-09 \pm 1.64e-09$	$5.1953e-12 \pm 2.14e-12$
Si	$-8.729e-05 \pm 2.43e-05$	$1.8175e-06 \pm 3.06e-07$	$-4.4084e-09 \pm 1.22e-09$	$3.962e-12 \pm 1.56e-12$
InAs	$4.5167e-06 \pm 5.92e-05$	$2.6904e-06 \pm 8.63e-07$	$-8.1426e-09 \pm 3.96e-09$	$8.3093e-12 \pm 5.77e-12$
InSb	$5.1128e-05 \pm 9.85e-05$	$4.5521e-06 \pm 1.25e-06$	$-1.1075e-08 \pm 3.88e-09$	0 ± 0

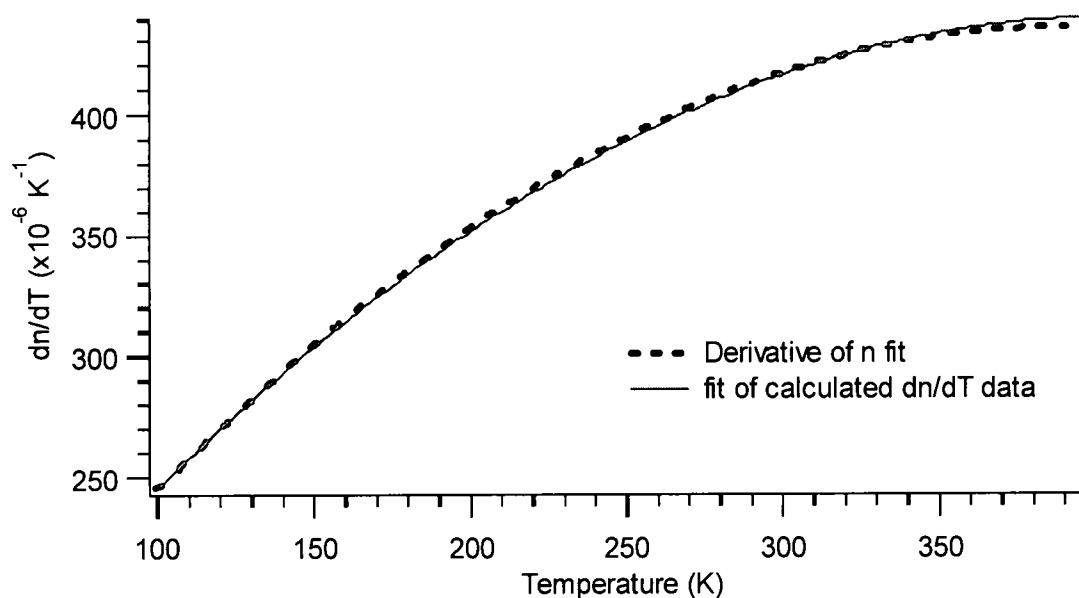


Figure 7.13: dn/dT vs. temperature for Ge using two methods.

Chapter 8

Conclusions

8.1 *Accomplishments*

The goal of this project was to build an experiment that could accurately measure the temperature-dependent index of refraction and thermo-optic coefficient of semiconductor materials for temperatures between room and cryogenic. This was accomplished for germanium, silicon, indium arsenide, and indium antimonide.

In all four cases, it was shown that the index of refraction and thermo-optic coefficient decreases as temperature decreases. For both sets of data, a polynomial was decided to be the best fitting function to be used to describe these relationships along with the actual graphical data collected. The project also provided a linear thermal expansion coefficient for each of these materials. This calculation is not as accurate as the index measurements but it is a decent rough estimate of the effect of temperature on thickness for any material in which greater studies on the subject have not yet been done.

In comparison to other experiments created for the measurement of index and thermo-optic measurements, this project had many advantages. This project

required a minimum amount of sample. All that was needed was a thin flat parallel wafer. While all the samples used at the point of this paper were approximately 1-2 mm thick, a sample as thin as a few hundred micron would have worked just as well though less interferometric peaks would occur across a set temperature range. The value of this is that newly created or just simply rare sample materials could be studied without collecting a large quantity. Along with that, a second advantage is that the sample can be studied using this method without causing any harm to the material itself. Therefore, no material is lost in this process either.

The experiment is also reasonably quick. Assuming the sample studied is flat-parallel, is not too lossy, and has a fairly temperature-independent transmission function at the studied wavelength, a calculation of the index and thermo-optic values could be accomplished in a week. Once aligned with one sample, the interferometers are aligned for any sample short of some quick and minor adjustments. The LaserMike requires a bit more alignment to be sure there is no back reflection in the system. This involves taking some data at a few different dewar positions and can take a few hours.

Finally, the experiment provides data for cryogenic temperatures. In comparison to previous works on this subject, very few have worked across this temperature range. For this reason, the experiment can be useful for not only newly created materials, but possibly many common materials that have not been studied below room temperature.

8.2 *Future Goals*

There are two major goals for the future of this project. The first is to study more materials. This project provides valuable information for any material that has not yet been studied. Specifically, ternary semiconductors such as InAsSb, MCTs, and InGaSb are of interest, as well as the effects of mixture concentrations on each material. Since this project provides a way to discern information about a newly created material without needing a large sample or having to cause any damage to it, it is essential for these kinds of materials.

The second goal is to measure and calculate the temperature-dependent index of refraction and thermo-optic coefficients for different materials using multiple wavelengths. Presently, information collected is valid for 10.591 μm . By taking data with multiple systems, a temperature and wavelength dependent index of refraction could be measured. This would provide the information needed to fit a material's Sellmeier equation. Specifically, a 1.34 μm Nd:YVO₄ laser and a 4.6-5.4 μm frequency-doubled CO₂ laser are planned to be added to the system in the near future.

To keep the project capable of moving quickly and easily, multiple lasers would have to be aligned to both the temperature-dependent Fabry-Perot interferometer and the angle-dependent Michelson/Fabry-Perot. Using a combination of flipper mirrors and beam blocks would make this possible. Figure 8.1 depicts the general setup used for this project at present with one other laser added to the system. M1 and M2 are flipper mirrors. In this present design, four experimental setups are possible. Table 8.1 describes each.

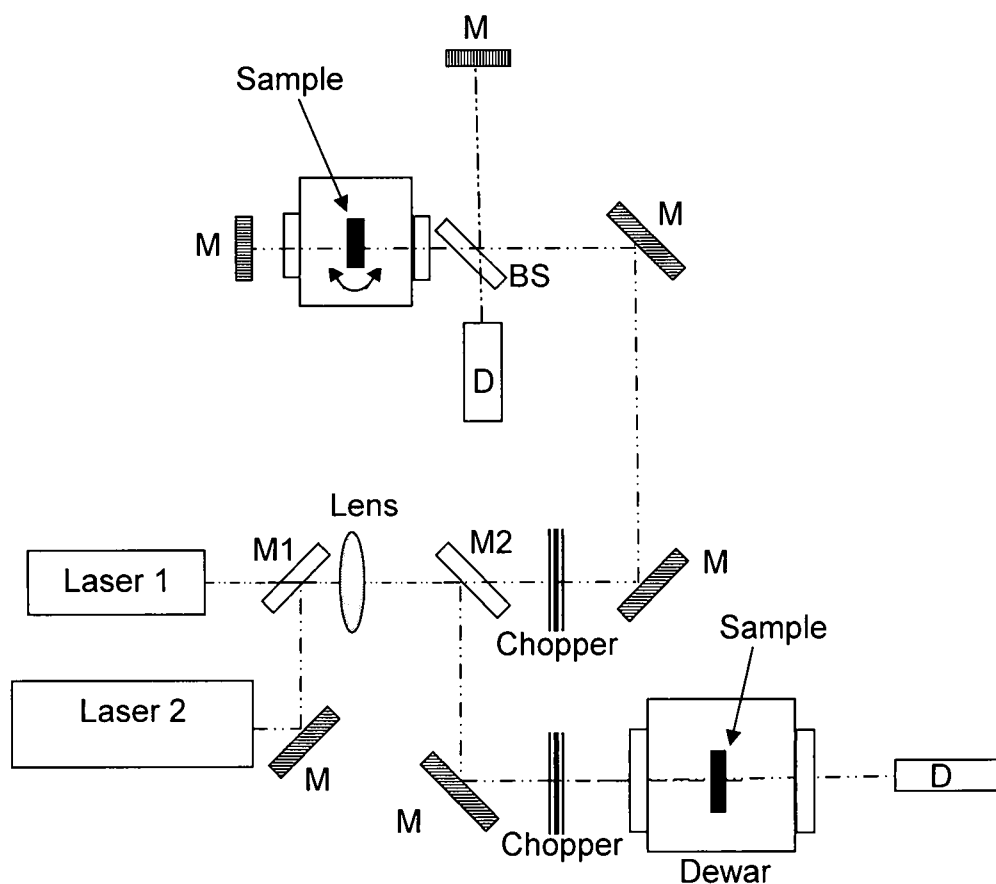


Figure 8.1: Future setup for both interferometers.

Table 8.1: Possible setups using two laser design for Project.

Cases	M1	M2
Temperature Dependent Fabry-Perot using Laser 1	Down	Up
Temperature Dependent Fabry-Perot using Laser 2	Up	Up
Angle Dependent Michelson/Fabry-Perot using Laser 1	Down	Down
Angle Dependent Michelson/Fabry-Perot using Laser 2	Up	Down

References

- [1] G. D. Gillen and S. Guha, "Use of Michelson and Fabry-Perot interferometry for independent determination of the refractive index and physical thickness of wafers", *Appl. Opt.* **44**(3), 344-347 (2005).
- [2] G. D. Gillen and S. Guha, "Refractive-index measurements of zinc germanium diphosphide at 300 K and 77 K by use of a modified Michelson interferometer", *Appl. Opt.* **43**(10), 2054-2058 (2004).
- [3] M. Born and E. Wolf, *Principles of Optics*, (Cambridge: University Press, 1999), p. 12-14, 190-192.
- [4] R.N. Singh, D.P. Juyal, J.S. Bhargava, K.M. Mathur. O.S. Nagar, and A.N. Bhattacharyya, "An accurate visual method for refractive index measurement in near infrared", *J. of Phys. E.* **4**, 283-285 (1971).
- [5] D.E. Aspnes and A.A. Studna, "Dielectric functions and optical parameters of Si, Ge, GaP, GaAs, GaSb, InP, InAs, and InSb from 1.5 to 6.0 eV", *Phy. Rev. B.* **27**(2), 985-1009 (1983).
- [6] S. Su, "A rapid and accurate procedure for the determination of refractive indices of regulated asbestos minerals", *American Mineralogist* **88**, 1979-1982 (2003).
- [7] J. Jewell, C. Askins, and I. D. Aggarwal, "Interferometric method for concurrent measurements of thermo-optic and thermal expansion coefficients", *Appl. Opt.* **30**(25), 3656-3660 (1991).
- [8] S. Waldenstrom and K.R. Naqvi, "A simple accurate alternative to the minimum-deviation method for the determination of the refractive index of a prism", *Am. J. Phys.* **46**(10), 1009-1011 (1978).
- [9] M. Deetlefs, K.R. Seddon, and M. Shara, "Neoteric optical media for refractive index determination of gems and minerals", *New J. Chem.* **30**, 317-326 (2006).

- [10] T. Dennis, E.M. Gill, and S.L. Gilbert, "Interferometric measurement of refractive-index change in photosensitive glass", *Appl. Opt.* **40**(10), 1663-1667 (2001).
- [11] J.A. McCaulley, V.M. Donnelly, M. Vernon, and I. Taha, "Temperature dependence of the near-infrared refractive index of silicon, gallium arsenide, and indium phosphide", *Phy. Rev. B.* **49**(11), 7408-7417 (1993).
- [12] H.G. Lipson, Y.F. Tsay, B. Bendow, and P.A. Ligor, "Temperature dependence of the refractive index of alkaline earth fluorides", *Appl. Opt.* **15**(10), 2352-2354 (1976).
- [13] P. Yu and M. Cardona, "Temperature Coefficient of the Refractive index of Diamond- and Zinc-Blende-Type Semiconductors", *Phys. Rev. B.* **2**(8), 3193-3197 (1970).
- [14] A.N. Pikhtin and A.D. Yas'kov, "Dispersion of the refractive index of semiconductors with diamond and zinc-blende structures", *Sov. Phys. Semicond.* **12**(6), 622-626 (1978).
- [15] F.L Pedrotti and F.J.L.S Pedrotti, *Introduction to Optics*, (Eaglewood Cliffs: Prentice Hall Inc, 1987), p. 290-291.
- [16] N. P. Barnes and M. S. Piltch, "Temperature-dependent Sellmeier coefficients and nonlinear optics average power limit for germanium", *J. Opt. Soc. Am.* **69**(1), 178-180 (1979).
- [17] H.W. Icenogle, Ben C. Platt, and William L. Wolfe, "Refractive indexes and temperature coefficients of germanium and silicon", *Appl. Opt.* **15**(10), 2348-2351 (1976).
- [18] Y.S. Touloukian, *Thermophysical Properties of Matter, The TPRC Data Series*, (New York: IFI/Plenum, 1975), p. 116-124.
- [19] G. Hawkins and R. Hunneman, "The temperature-dependent spectral properties of filter substrate materials in the far-infrared (6-40 μm)", *Infrared Phys. and Tech.* **45**(1), 69-79 (2004).
- [20] M. Levinshstein, S. Rumyantsev, and M. Shur, *Handbook series on Semiconductor Parameters, Volume 1*, (Singapore: World Scientific Publishing, 1996), p. 2,34,148,191.
- [21] V. Kumar and B.S.R. Sastry, "Thermal Expansion Coefficient of Binary Semiconductors", *Cryst. Res. Technol.* **36**(6), 565-569 (2001).

R002S88689

The HF Group

Indiana Plant

T 052545 F 11 00



6/8/2006